AD-A133 873 RAPID SOLIDIFICATION PROCESSING AND POWDER METALLURGY OF AL ALLOYS(U) ILLINOIS UNIV AT URBANA DEPT OF METALLURGY AND MINING ENGINEERING H L FRASER 19 SEP 83 1/1

UNCLASSIFIED AFOSR-TR-83-0826 AFOSR-82-0186 F/G 11/6 NL

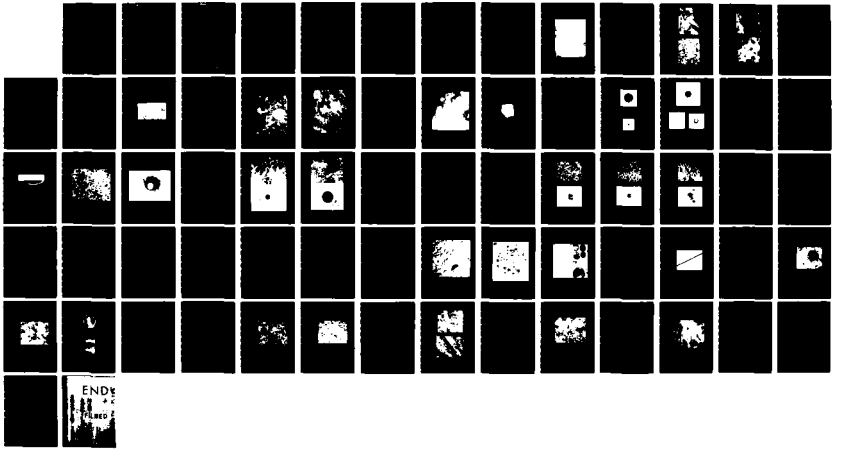

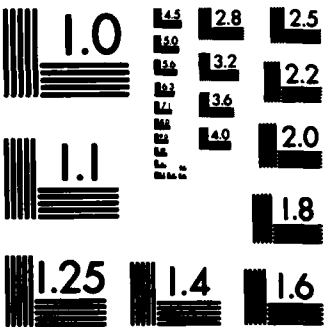

MICROCOPY RESOLUTION TEST CHART
NATIONAL BUREAU OF STANDARDS-1963-A

UNCLASSIFIED

SECURITY CLASSIFICATION OF THIS PAGE (When Data Entered)

AD-A133873

REPORT DOCUMENTATION PAGE

READ INSTRUCTIONS BEFORE COMPLETING FORM

1. REPORT NUMBER: AFOSR-TR- 83-0826	2. GOVT ACCESSION NO.: AD-A133873
3. RECIPIENT'S CATALOG NUMBER:	
4. TITLE (and Subtitle): Rapid Solidification Processing and Powder Metallurgy of Al Alloys	5. TYPE OF REPORT & PERIOD COVERED: annual
	6. PERFORMING ORG. REPORT NUMBER:
7. AUTHOR(s): Hamish L. Fraser	8. CONTRACT OR GRANT NUMBER(s): AFOSR-82-0186
9. PERFORMING ORGANIZATION NAME AND ADDRESS: University of Illinois, Dept. of Metallurgy 1304 W. Green, Urbana, IL 61801	10. PROGRAM ELEMENT, PROJECT, TASK AREA & WORK UNIT NUMBERS: 61102F 2306/A1
11. CONTROLLING OFFICE NAME AND ADDRESS: Air Force Office of Scientific Research Bolling AFB, Bldg. 410, Washington, DC 20332	12. REPORT DATE: 9/19/83
	13. NUMBER OF PAGES: 66
14. MONITORING AGENCY NAME & ADDRESS(if different from Controlling Office)	15. SECURITY CLASS. (of this report): unclassified
	15a. DECLASSIFICATION/DOWNGRADING SCHEDULE:

16. DISTRIBUTION STATEMENT (of this Report)

This document has been approved for public release; its distribution is unlimited.

17. DISTRIBUTION STATEMENT (of the abstract entered in Block 20, if different from Report)

18. SUPPLEMENTARY NOTES

19. KEY WORDS (Continue on reverse side if necessary and identify by block number)

Rapid solidification processing of Al-alloys, powder metallurgy, dynamic powder compaction

20. ABSTRACT (Continue on reverse side if necessary and identify by block number)

On reverse side

DD FORM 1 JAN 73 1473 EDITION OF 1 NOV 65 IS OBSOLETE

UNCLASSIFIED

SECURITY CLASSIFICATION OF THIS PAGE (When Data Entered)

During the first period of performance, three tasks have been undertaken. These involve first a study of the specific microstructural changes that accompany rapid solidification of a number of Al alloys together with a determination of the thermal stability of these microstructures, second the production of rapidly solidified particulate and third the use of dynamic powder compaction (DPC) for the consolidation of rapidly solidified particulate in the absence of prolonged thermal excursions.

A number of alloys have been rapidly solidified using laser surface melting and melt-spinning and in each case the observed microstructure has been interpreted in terms of the undercooling achieved during processing. Of interest is the transition from zone A (very refined) to zone B (coarse) microstructures and this transition is thought to be caused by variations in undercooling where large values of this parameter favor formation of zone A. The microstructures of as rapidly solidified and heat treated samples of Al-8Fe-2Mo and Al-7.9Fe-2.9Ce (wt%) have been compared, and, in both conditions, the Mo containing alloy exhibits a more refined structure and a greater resistance to thermal decomposition. Hardness measurements are in accord with this, and indicate that the Al-8Fe-2Mo possesses higher strengths than the Ce containing alloy both in the as-solidified and heat treated conditions. It appears that the superior hardness values may be associated with the extremely refined dispersion of (metastable) intermetallic phases present in the inter-cellular regions of the zone A microstructure.

Rapidly solidified (gas atomized) powders of 7091 have been consolidated using DPC. It has been shown that bulk samples may be produced that are close to theoretical density. The microstructure of these compacts is dendritic, and observations made of many prior particle regions are consistent with the occurrence of local melting during shock wave propagation which is thought to be involved in the mechanism of consolidation. Bulk pieces have been heat treated at both 523 K and 723 K, so that any possible cavitation or void formation caused by the decomposition of the hydrated oxide known to be present on the powders may be observed. No such behavior was, in fact, seen; the microstructure of these samples has been characterized.

First Annual Technical Report on

Rapid Solidification Processing and Powder Metallurgy of Al Alloys

AFOSR Grant No: AFOSR-82-0186

Progress in Research during the period

15th April to 14th April 1983

submitted by:

Hamish L. Fraser 359-56-6563
Department of Metallurgy
University of Illinois
1304 W. Green
Urbana, IL 61801 (217) 333-1975

Abstract

During the first period of performance, three tasks have been undertaken. These involve first a study of the specific microstructural changes that accompany rapid solidification of a number of Al alloys together with a determination of the thermal stability of these microstructures, second the production of rapidly solidified particulate and third the use of dynamic powder compaction (DPC) for the consolidation of rapidly solidified particulate in the absence of prolonged thermal excursions.

A number of alloys have been rapidly solidified using laser surface melting and melt-spinning and in each case the observed microstructure has been interpreted in terms of the undercooling achieved during processing. Of interest is the transition from zone A (very refined) to zone B (coarse) microstructures and this transition is thought to be caused by variations in undercooling where large values of this parameter favor formation of zone A. The microstructures of as rapidly solidified and heat treated samples of Al-8Fe-2Mo and Al-7.9Fe-2.9Ce (wt%) have been compared, and, in both conditions, the Mo containing alloy exhibits a more refined structure and a greater resistance to thermal decomposition. Hardness measurements are in accord with this, and indicate that the Al-8Fe-2Mo possesses higher strengths than the Ce containing alloy both in the as-solidified and heat treated conditions. It appears that the superior hardness values may be associated with the extremely refined dispersion of (metastable) intermetallic phases present in the inter-cellular regions of the zone A microstructure.

Rapidly solidified (gas atomized) powders of 7091 have been consolidated using DPC. It has been shown that bulk samples may be produced that are close to theoretical density. The microstructure of these compacts is dendritic, and observations made of many prior particle regions are consistent with the occurrence of local melting during shock wave propagation which is thought to

be involved in the mechanism of consolidation. Bulk pieces have been heat treated at both 523 K and 723 K, so that any possible cavitation or void formation caused by the decomposition of the hydrated oxide known to be present on the powders may be observed. No such behavior was, in fact, seen; the microstructure of these samples has been characterized.

1. Introduction

The program involves a study of rapid solidification processing and powder metallurgy of Al alloys. During the first year, three tasks have been undertaken. The first of these has been concerned with a determination of the specific microstructural changes that occur as a result of rapid solidification in a number of Al alloys. For this purpose, laser surface melting and melt-spinning have been used to provide convenient means for the production of small volumes of material. The thermal stability of these microstructures has also been established by isochronal and isothermal anneals. Of special interest in this section of the program is a comparison of the changes in microstructure between the ternary alloys similar to Al-8Fe-2Mo and Al-8Fe-3Ce which have been the subject of much recent work (Pratt and Whitney Aircraft and ALCOA, respectively).

The second task has involved the production of rapidly solidified particulate. Three methods of preparation have been used, namely laser spin atomization, centrifugal atomization and melt-spinning where, in this latter approach, ribbons are subsequently reduced to particulate. The third task is aimed at the application of dynamic powder compaction to the consolidation of rapidly solidified Al alloys. In this part of the research, the main interest is in compaction of material with the minimum of thermal excursions, so that bulk pieces of various alloys possessing refined microstructures may be produced. This work has initially been concerned with compaction of powders of 7091.

2. Microstructural Analysis of Rapidly Solidified Al-Ni, Al-Mo, Al-Fe Al-Fe-Mo, Al-Fe-Ce Alloys

The first part of the present program involves a study of the microstructures of various Al-alloys following rapid solidification (RS). Two

techniques have been used to effect RS in these alloys, one involving laser surface melting and the other melt spinning. Most of the work has involved the former, since this is an extremely convenient means of producing small volumes of material with which to study specific microstructural changes. As work has progressed, more attention is now being focussed on melt spinning since not only is this another relatively easy means of producing rapidly solidified material, but also the ribbon may be reduced to particulate and subsequently compacted into bulk pieces. Progress in this area, which appears already to involve exciting results will be reported in the second annual report. The results of work on rapidly solidified powders are detailed below, but this more difficult and time consuming approach (i.e. a study of the powders themselves) to the evaluation of the effects of RS on microstructure has not been employed.

2.1 Al-Ni Alloys

Two alloys taken from the Al-Ni binary system have been subjected to laser surface melting. Their compositions are nominally 3.3 and 8.0 at%, respectively. An eutectic mixture, consisting of α-Al and the intermetallic Al_3Ni, forms at a liquid composition of $\sim$ 2.7 at% Ni; the present alloys are, therefore, of hypereutectic compositions. An optical micrograph of a transverse cross-section of the laser surface melted region of the 8.0 at% Ni alloy is shown in Fig. 1. Within the melt-pool itself, various regions of differing contrast may be discerned. First, at the boundary between the underlying substrate and melt-pool, there appears to be material which has only partially melted. This is thought to be due to the fact that the absorbed heat was not sufficient to melt the relatively high temperature phase, Al_3Ni, but did indeed melt the surrounding phase, α-Al (solid solution). There are two other regions of the melt-pool which are apparent, one exhibiting little or no contrast, the other marked contrast. Jones[1] has referred to these features of optical micrographs of rapidly solidified Al alloys as zone A and zone B,

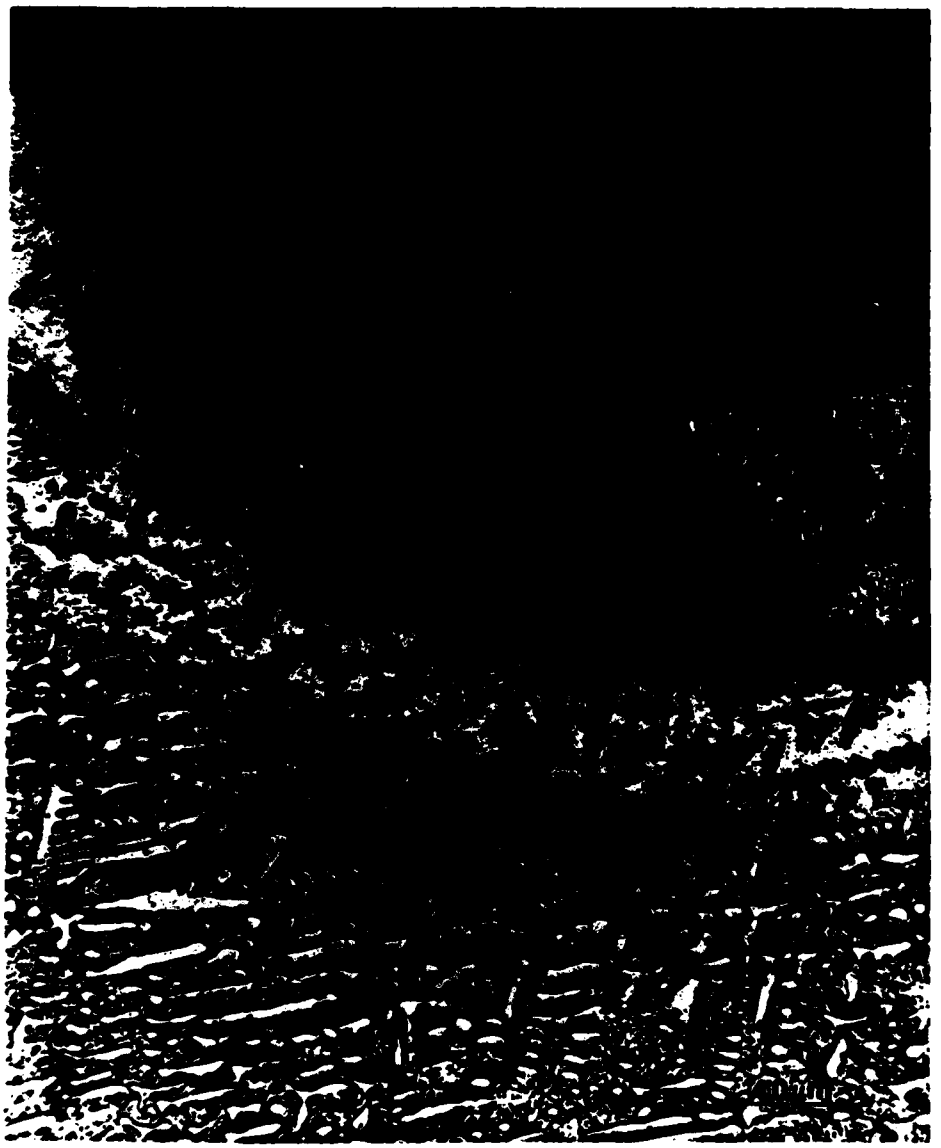

1) Optical micrograph of the laser surface melted region of an Al-8at%Ni alloy. Note varying contrast in the melt pool region representing zone A and zone B microstructures.

respectively. The occurrence of zone A in a given microstructure is thought to be very significant, since the lack of contrast has been attributed to a very fine scale distribution of phases, which would be a direct result of RS. In the present study, this has been shown to be the case, and transmission electron micrographs (taken from samples) of zone A and zone B are presented in Figs. 2 and 3, respectively. For the 8.0 at% alloy, zone A (Fig. 2) is found to consist of a fine lamellar microeutectic of spacing ~ 400Å. The two phases present are found to be α-Al and Al_3Ni, this being deduced from selected area diffraction studies and energy dispersive x-ray spectroscopy (EDS) performed in the scanning transmission electron microscope (STEM). Zone B, however, is found to be a somewhat coarser distribution of the same phases, except in this case it appears that during solidification, primary dendrites of Al_3Ni are formed.

When the more dilute alloy (3.3 at%) is subjected to laser surface melting, usually only zone A is seen in optical micrographs of the melt-pool (e.g. Fig. 4). The microstructure of zone A in this alloy is, however, markedly different from that in the more concentrated material (discussed above), and as shown in Fig. 5, consists of a cellular microstructure where cells of α-Al supersaturated in Ni are surrounded by Al_3Ni.

These various observations, namely formation of zone A and zone B, and the change in zone A microstructure (from cells to a lamellar microeutectic) with composition may be explained with reference to the schematic phase diagram shown in Fig. 6. In essence, the various microstructures that form may be interpreted on the basis of the degree of local undercooling experienced by the liquid at the rapidly advancing solid/liquid interface. Consider first the solidification of liquid in the melt-pool of the more concentrated alloy (8.0 at%). Because of the large temperature gradients established by rapid heat extraction through the base metal, a relatively large degree of undercooling may be developed during surface melting and regrowth, such that the temperature of the liquid at the

2) Transmission electron micrograph of the zone A region of the specimen shown in figure 1 (At-8at%Ni), showing the fine microeutectic typical of the zone A microstructure in the higher Ni alloy.

3) Transmission electron micrograph of the zone B region of the specimen shown in figure 1 (Al-8at%Ni).

4) Optical micrograph of the laser surface melted region of an Al-3.3at%Ni alloy. Note the absence of zone B regions.

5) Transmission electron micrograph of the zone A region of the specimen shown in figure 4 (Al-3.3%Ni). Note the difference between the cellular nature of this microstructure and the microeutectic formed in the Al-8at%Ni alloy.

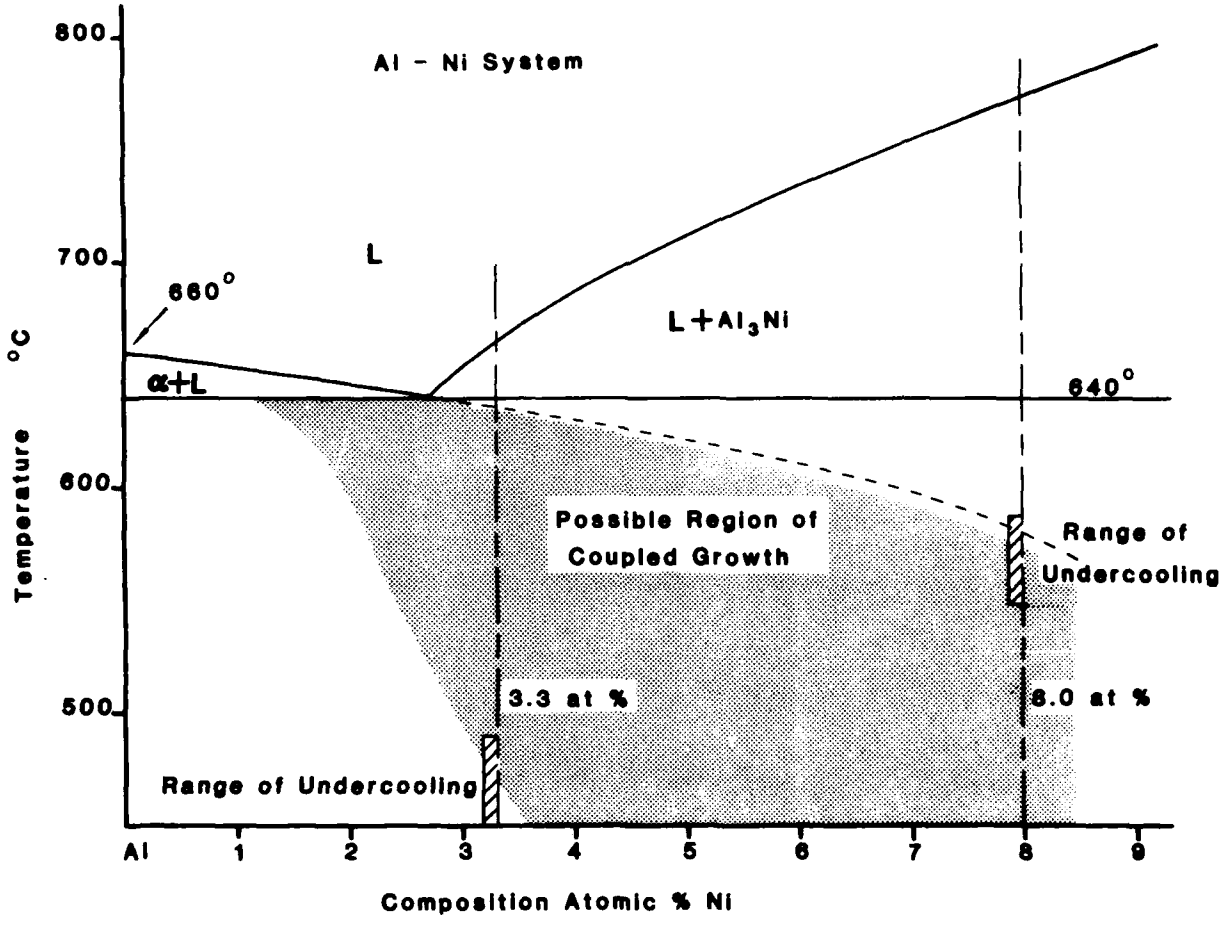

6) Al rich side of the Al-Ni equilibrium phase diagram showing the compositions of the two alloys studied and a possible configuration of the coupled growth region for the eutectic.

interface may fall below that of the extended hypoeutectic liquidus curve. When this occurs, it is thought that a change in the mode of solidification results such that precipitation of the α-phase occurs first rather than the Al_3Ni. Furthermore, it has been postulated[2] that for the case of an eutectic mixture involving a faceted phase (e.g. Al_3Ni), the zone of coupled growth is asymmetric, and shifts towards the faceted phase as growth rate (or undercooling) is increased. Such an asymmetric coupled zone is shown schematically in Fig. 6, and it is proposed here that this region of coupled growth lies very close to the extended hypoeutectic liquidus curve. In this case, if sufficient undercooling (~ 200°C) is achieved, the mode of solidification of liquid at the advancing interface is expected to change from that involving the precipitation of primary Al_3Ni to one involving coupled growth, i.e. a microeutectic mixture. This is indeed observed in the alloy of composition 8.0 at% Ni, where extensive regions of zone A are formed (Figs. 1,2). The presence of zone B, involving large dendrites of Al_3Ni, adjacent to zone A is now simply understood in terms of a small variation of undercooling such that the local liquid temperature is raised slightly above the extended hypoeutectic liquidus curve. Such variations in undercooling are to be expected in these experiments.

The formation of the cellular microstructure of zone A in the more dilute alloy (3.3 at% Ni) may also be understood on the same basis. Thus, the local undercooling of liquid at the advancing interface will be such that, at this composition, solidification will occur at temperatures much below the extended hypoeutectic liquidus curve. There is, then, no tendency for zone B formation (involving primary Al_3Ni precipitation). However, since this alloy composition is very close to that of the eutectic, and the region of coupled growth is expected to be asymmetrically shifted toward the faceted phase, it is highly likely that solidification will occur in an uncoupled fashion, involving cells

of α-Al together with intercellular Al_3Ni. This is indeed the most frequent observation (Fig. 5). Occasionally, some microeutectic is formed, and this again may be understood on the basis of a small local decrease in undercooling such that solidification may, once again, occur in the region of coupled growth.

The arguments presented above concerning the mechanism of formation and microstructural character of zones A and B are based on two premises, one that there is sufficient undercooling during solidification that for the most part precipitation of primary Al_3Ni is suppressed, and the other that the region of coupled growth is asymmetric and shifted toward the faceted Al_3Ni phase. However, the compositions chosen appear to represent two very different extremes such that in the dilute alloy, a cellular microstructure results, whereas in the more concentrated alloy, a fine lamellar eutectic was observed. Present work is aimed at substantiating the model and involves the laser surface melting of an Al-6.0 at% Ni alloy, where, on the basis of the arguments described above, it is predicted that the microstructure will be entirely zone A, and consist of a refined lamellar microeutectic mixture of α-Al and Al_3Ni.

2.2 Al-Mo Alloys

Two alloys taken from the Al-Mo system were prepared, namely 0.5 and 1.46 at% Mo. As-cast samples were subjected to laser surface melting, and additionally melt-spun ribbons of both compositions were produced.

i) Microstructures of Laser Surface Melted Samples

A scanning electron micrograph of a transverse section of a melt-pool in Al-1.46 at% Mo is shown in Fig. 7. This image is recorded in the backscattered electron compositional mode. Therefore, changes in contrast represent variations in composition such that the lighter contrast regions correspond to enrichment of heavier elements. Thus, in the as-cast unmelted parts of the sample, the light dendritic structures are very rich in Mo, this being the primary Al_5Mo phase; the nature of this phase was determined by both selected

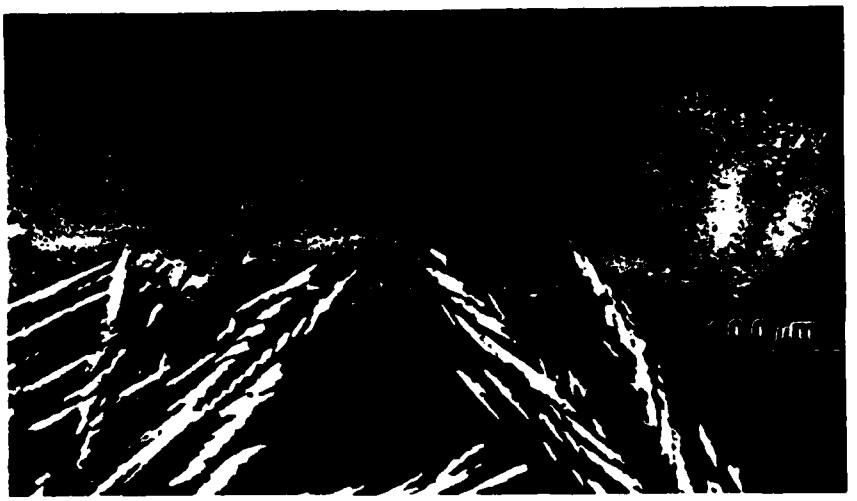

7) Scanning electron micrograph of the laser surface melted region of an Al-1.46at%Mo alloy taken using the backscattered electron compositional mode. Note the light and dark areas within the melt pool indicating chemical inhomogeneity.

area diffraction studies and EDS measurements. In the melt pool, a variation in contrast is seen to occur, and this may be interpreted as an inhomogeneous distribution of Mo in the melted region. The reason for this is presumably due to the high melting point of the alloy at this concentration, so that the superheat produced during laser surface melting may be insufficient to cause complete melting and elemental mixing prior to rapid solidification. If this is indeed the case, then there should be differences in the composition of the matrix phase in thin foils of the melt-pool. Typical microstructures of thin foils taken from the laser melted regions of the two alloys (0.5 at% and 1.46 at% Mo) are shown in Fig. 8. Essentially, the microstructure of the more dilute alloy consists of a single phase of α-Al, supersaturated with Mo to the alloy composition, 0.5 at%. The matrix phase in the microstructure of the more concentrated alloy is also supersaturated with Mo, but as mentioned above, the Mo is not expected to be homogeneously distributed. A large number of EDS spectra taken from a variety of specimens was recorded, and using elemental standards to permit compositional determinations to be performed, a range of matrix compositions was found between 0.1 - 2.4 at% Mo. It should be noted that this range extends above the alloy composition (1.46 at%), and emphasizes the fact that an inhomogeneous distribution of Mo exists. However, the present results show that during laser surface melting, a relatively large supersaturation of Mo may be trapped in the Al solid solution, the largest value reported here (2.4 at%) being consistent with the work of Polesya and Stepina[3].

In the microstructures of laser melted samples of both alloys, Fig. 8, a small number of second phase particles may be seen. It is thought that these particles are in fact small pieces of the preexisting dendrites of Al_5Mo, which have persisted in the melt-pool during processing. This view is consistent with that described above, where the origin of the inhomogeneous distribution of Mo is thought to involve the development of an insufficient degree of super-

8a) Transmission electron micrograph of laser surface melted Al-0.5at%Mo alloy. Beam direction close to [011].

8b) Transmisson electron micrograph of laser surface melted Al-1.46at%Mo alloy. Beam direction close to [112].

heat necessary to permit complete melting and elemental mixing prior to solidification.

ii) Microstructures of Melt-Spun Ribbon

A significant difference between laser surface melting and melt-spinning involves the degree of superheat generated in the melt before solidification occurs. Thus, as mentioned above, this can be limited in the case of surface melting. However, this is not the case in melt-spinning, and complete melting of all phases present and mixing of the elemental components can be achieved in the liquid state. In view of the results described above, where it is shown that up to 2.4 at% Mo may be trapped, it might be expected that the microstructure of melt-spun ribbons of both alloys would consist simply of supersaturated Al solid solutions. This is indeed the case for the more dilute alloy, but in the Al-1.46 at% Mo alloy, the microstructure of the melt-spun ribbon is found to consist of two phases, as shown in Fig. 9. A cursory investigation aimed at identifying the nature of these precipitates using selected area diffraction showed that they were not any of the known intermetallic compounds involving Al and Mo (i.e. $Al_{12}Mo$, (Al_7Mo), Al_5MO, (Al_4Mo) or Al_3Mo, where parentheses indicate a metastable phase). Consequently, a detailed structural analysis was undertaken involving convergent beam electron diffraction (CBED) and EDS.

At first, thin foils were electrochemically polished and any resultant surface layers were removed by Ar ion sputtering in an Auger electron spectrometer (AES). EDS spectra were recorded and quantification was achieved using pure elemental standards. The composition of the phase was found to correspond approximately to Al_4Mo. The precipitate shown in Fig. 10 was examined using CBED following the method of Buxton, et al.[4]. However, it should be noted that there appears to be significant faulting or twinning in the precipitates and this may lead to an ambiguity in interpretation of some of

9) Transmission electron micrograph of Al-1.46at%Mo alloy melt-spun ribbon showing precipitates and associated dislocation structure. Beam direction close to [101].

10) Transmission electron micrograph of precipitate in Al-1.46at%Mo ribbon. This precipitate was used in the convergent beam diffraction studies. The electron probe was focused in the unfaulted region in the upper left corner.

the patterns. Bearing this in mind, diffraction patterns were obtained with the electron beam accurately aligned parallel to the precipitate zone axes [100] and [111], and these are presented in Figs. 11 and 12, respectively. In each case, the projection diffraction and whole pattern symmetries may be deduced, and in the case of Fig. 12, the bright field (HOLZ) symmetry for the [111] zone axis may also be determined. These various symmetries are listed in Table 1, and it is possible to include also the deduced diffraction groups corresponding to the pattern symmetries, using the tables in ref. 4. The possible crystal point groups which correspond to these deduced diffractions are given in Table 2. It can be seen that the m3m is the only consistent point group.

Zone axis	Pattern Symmetries			Deduced diffraction group
	Projection diffraction	Whole pattern	Bright field	
100	4 mm	4 mm	----	4 mm, $4mml_R$
111	6 mm	3 m	3 m	6_Rmm_R

Table 1. Pattern symmetries recorded from the two zone axes [100] and [111]

Zone Axis	Deduced diffraction groups	Possible Point Groups			
		4 mm	4/mmm	m3m	2mm
100	4mm	x			
	$4mml_R$		x	x	
111	6_Rmm_R			x	

Table 2. Possible point groups corresponding to the deduced diffraction groups

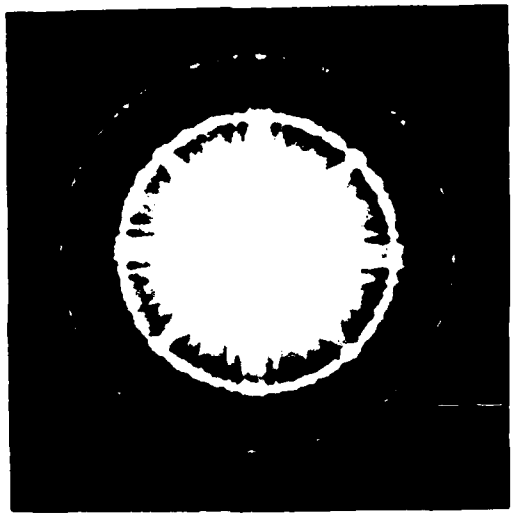

a)

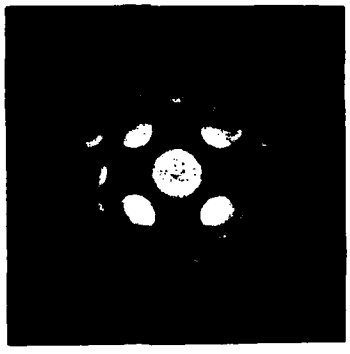

b)

11) Electron diffraction patterns obtained from the precipitate shown in figure 10, [100] zone axis.
    a) whole pattern
    b) zero order pattern

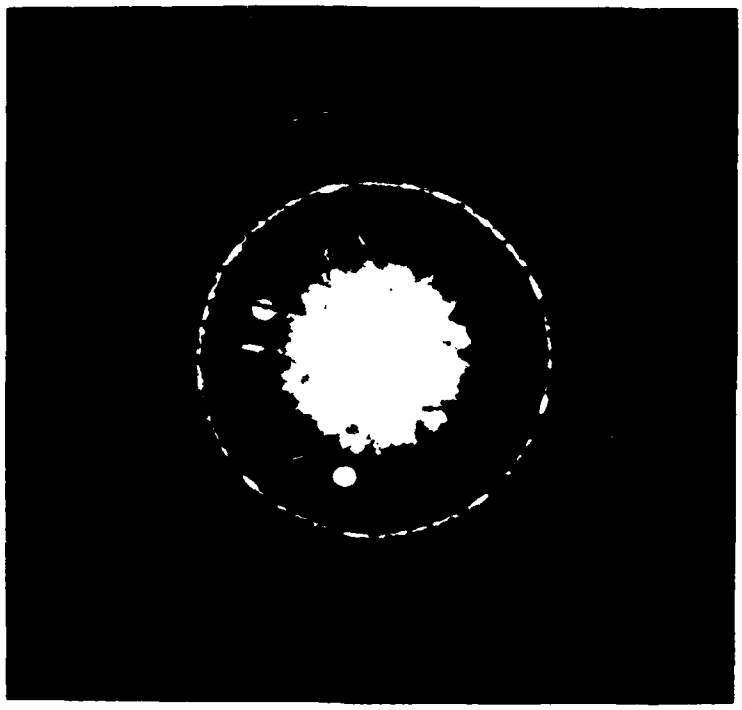

a

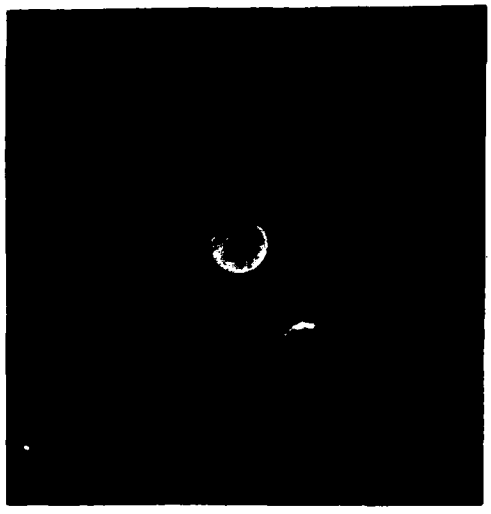

b

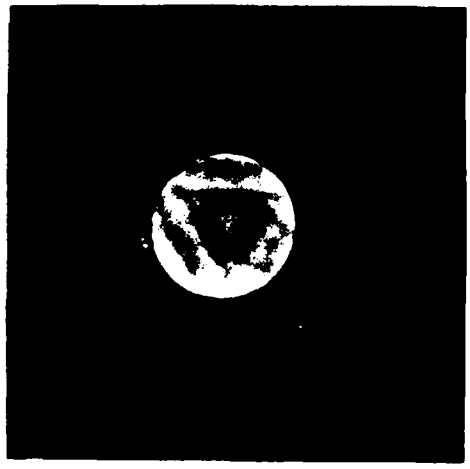

c

12) Electron diffraction patterns obtained from the precipitate shown in figure 10, [111] zone axis
a) whole pattern
b) zero order pattern
c) bright field pattern

The type of unit cell (i.e. primitive, body- or face-centered) may be determined by projecting the reflections contained in the first and second order Laue zones back into the zero order zone of the [100] pattern. When this is done, a face centered reciprocal lattice cell results, corresponding to a body centered real lattice cell. From a combination of this information, the deduced point group and a knowledge of the absent reflections, it is possible to determine the space group of the compound. In the present case, Im3m appears to be the only consistent space group. The lattice parameter has been determined from the diffraction patterns as being given by a = 5.39 Å. The occurrence of such a phase, Al_4Mo, possessing the space group Im3m, has not been previously reported in the literature, and is presumably a metastable phase formed during rapid quenching of the alloy.

2.3 Al-Fe, Al-Fe-Mo, Al-Fe-Ce Alloys

The microstructures of rapidly solidified alloys based on the Al-Fe binary system have been studied previously[1,5,6]. This has led to the development of two ternary alloys Al-8Fe-2Mo (Pratt and Whitney Aircraft) and Al-8Fe-3Ce (ALCOA) where the compositions are expressed in wt.%. A part of the present program involves a comparison of microstructures of rapidly solidified samples of the binary Al-Fe alloy system, and these two ternary alloys. The compositions have been chosen so that the atomic concentrations of solute in each alloy will be identical, and, arbitrarily, this value has been chosen to be the same as that corresponding to the composition Al-8Fe-2Mo (wt%), i.e. the combined solute composition in each alloy is 4.7 at%. In the ternary alloys, the atomic concentration of Fe is 4.1%, and those of Mo and Ce are both 0.6%, and so the alloy compositions in wt% are given by Al-9.2Fe, Al-8Fe-2Mo and Al-7.9Fe-2.9Ce. These alloys will be referred to as AlFe, AlFeMo and AlFeCe, respectively.

There are three phases of the present study; the first is a determination of the microstructure of rapidly solidified samples where for convenience laser

surface melting is employed. The second is a set of experiments aimed at a determination of the thermal stability of the microstructures, and the third involves hardness measurements of the as-solidified and heat treated materials to give an indication of the response of mechanical properties to this type of processing. The results of each phase of the work will be presented first, followed by a general discussion.

2.3.1 Microstructures of Rapidly Solidified Alloys

An optical micrograph of the laser surface melted region of the binary alloy AlFe is shown in Fig. 13. The featureless contrast associated with the melted region permits this microstructure to be termed Zone A, following Jones[1] (and as discussed in section 2.1 above). A TEM micrograph illustrating the microstructure of this melted region is shown in Fig. 14, and it is evident that zone A in this alloy consists of a fine cellular structure, where the cell diameter is ~ 0.1 μm. Diffraction and EDS studies reveal that the cells are based on α-Al, and there is evidently a Fe rich second phase at the intercellular regions. A selected area diffraction pattern taken from a sample containing zone A is shown in Fig. 15. The relatively diffuse rings of intensity are produced by the second phase, this being shown by dark field imaging from a section of one of the rings. It can be concluded from the continuous nature of these diffuse rings that the second phase precipitation in the intercellular regions is extremely fine and randomly oriented. It has not been possible to uniquely identify the nature of these precipitates because of their extremely fine size. The interplanar spacings have been determined from measurements of the spacings of the rings, and at best these may be loosely indexed on the basis of a cubic structure, following Jacobs, et al.[6] with lattice parameter given by a ~ 3.6Å.

An important aspect of the rapidly solidified microstructure is the degree of elemental segregation that has occurred. This can be determined by positioning the electron probe on or close to the center of a number of cells,

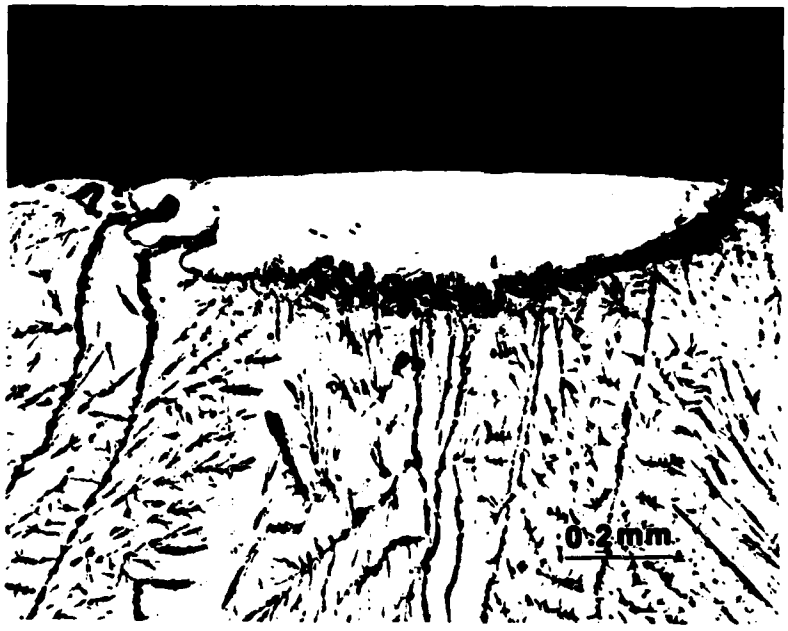

13) Optical micrograph of laser surface melted region of the AlFe binary alloy. Note that the entire melted region is featureless indicating the presence of the zone A microstructure.

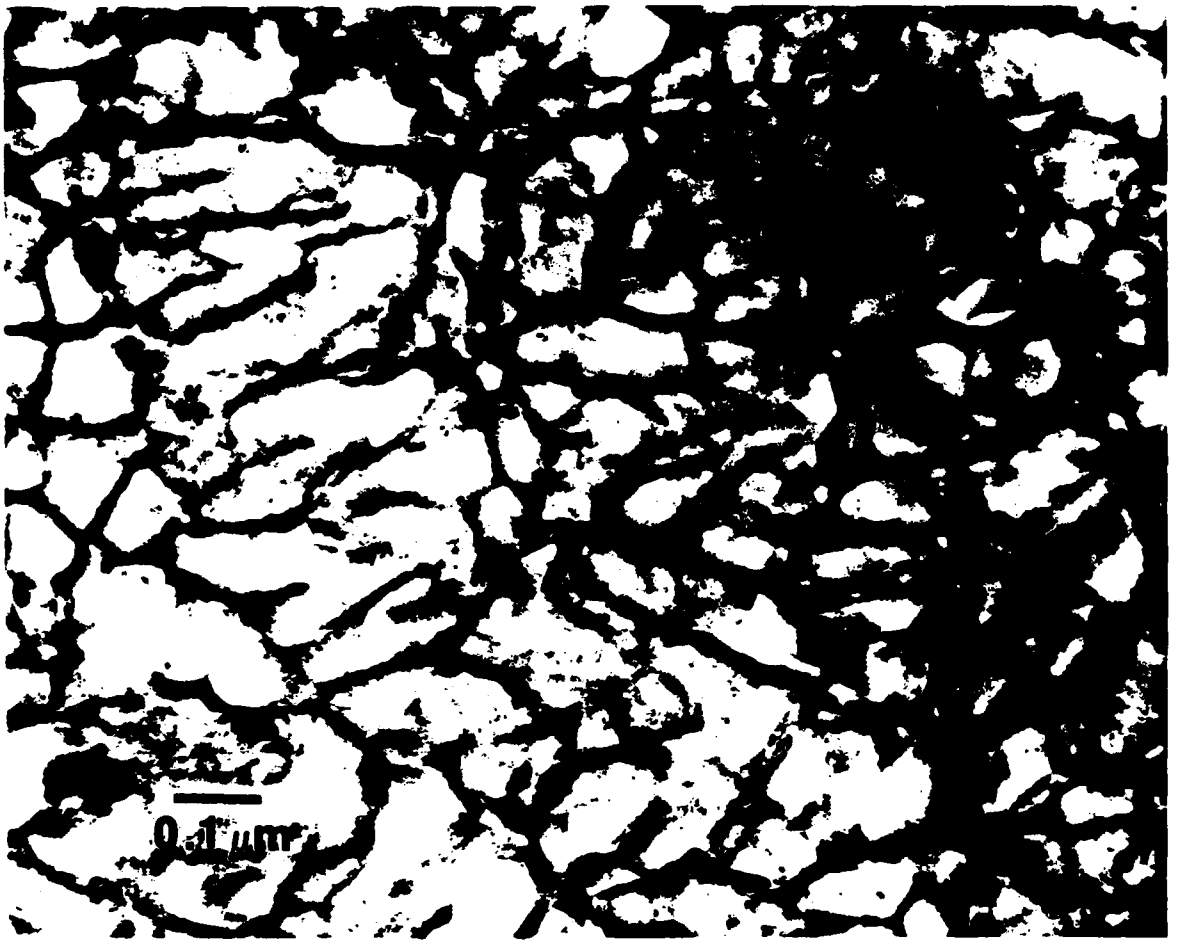

14) Transmission electron micrograph of the laser melted region of the AlFe alloy specimen shown in figure 13.

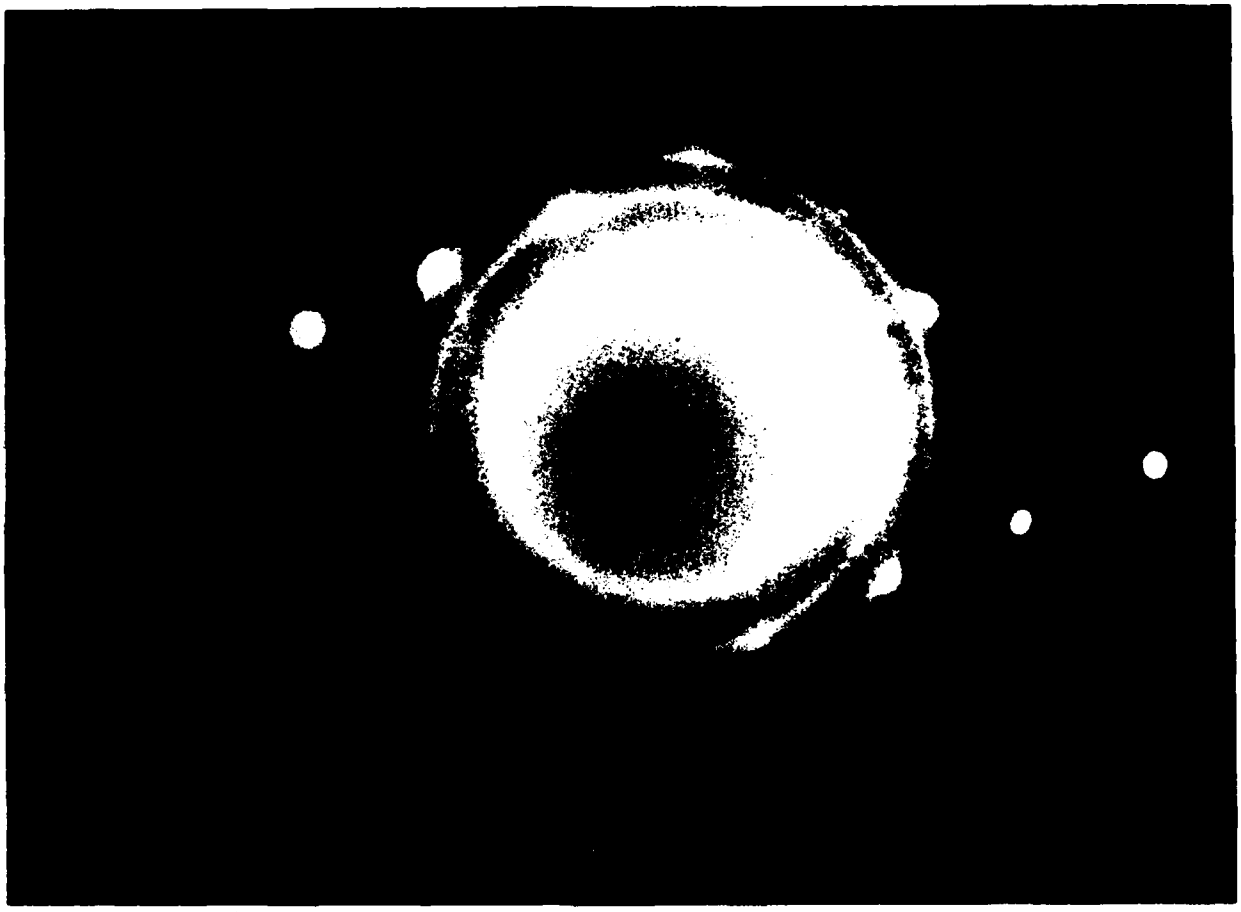

15) Selected area diffraction pattern from the specimen shown in figure 14 (AlFe binary). Note the presence of diffracted rings indicating an extremely fine, randomly oriented dispersion of second phase particles.

and recording the resulting EDS spectra, from which compositional information may be deduced. This has been done on foils that have first been subjected to Ar ion sputtering to remove the surface layers which result from sample preparation. In this experiment, compound sample standards were used for the purposes of quantification, and it was found that on average, cells in rapidly solidified AlFe contain ~ 3.86 at% Fe.

The microstructures and typical selected area diffraction patterns of thin foils taken from samples of rapidly solidified AlFeMo and AlFeCe are shown in Fig. 16 and Fig. 17, respectively. The microscope and diffraction pattern shown in Fig. 16 (AlFeMo) may be compared with those in Fig. 14 and Fig. 15 (AlFe), and it is immediately apparent that there is very little difference in either the microstructure or the nature of the second phase in rapidly solidified AlFe and AlFeMo. This is not the case when Fig. 17 is compared with either Figs. 14 and 15 or Fig. 16, and it seems that for AlFeCe while the cell diameter is still ~ 0.1 μm, the second phase is precipitated in a more discreet fashion. A close examination of the diffraction pattern in Fig. 17(b) reveals that the rings are much less diffuse than in Figs. 15 or 16(b), and are composed of a large number of individual diffraction maxima. It may be concluded that in the Ce containing alloy, the intercellular precipitation is somewhat coarser than in either the binary or Mo containing alloys, and dispersed correspondingly in a less random fashion.

The compositions of the cells have been determined in the same manner as described above using EDS. A comparison of the spectra recorded from the cells of AlFeMo and AlFeCe is shown in Fig. 18. In the preparation of this data, the Al K peaks have been normalized to one another, and are not plotted in Fig. 18; the various peak heights do, then, imply real changes in composition. The data have been quantified as before and the various cell compositions are listed in Table 3.

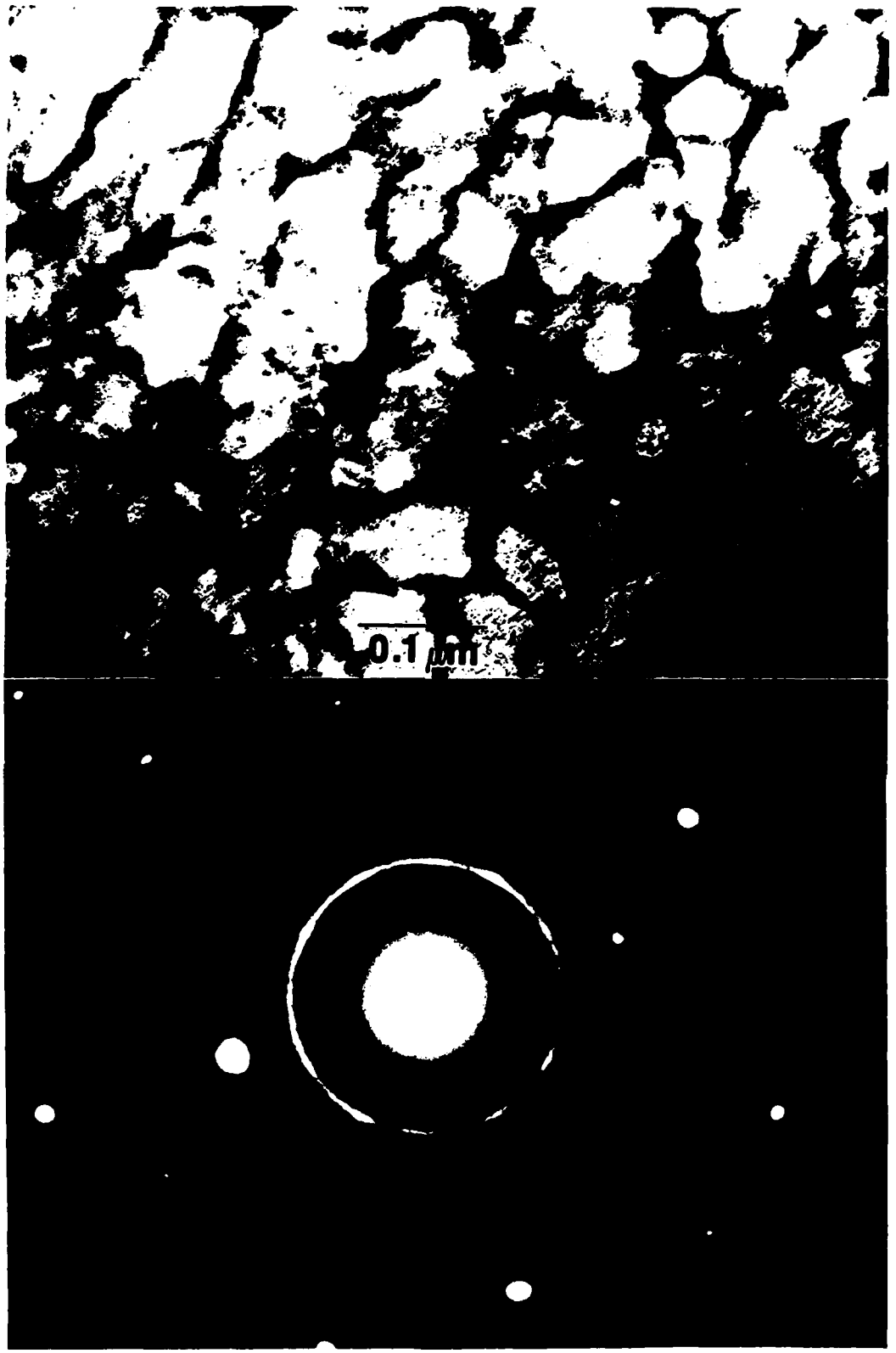

16) Transmission electron micrograph (a) and associated selected area diffraction pattern (b) of the laser melted AlFeMo alloy. Note the similarity of the microstructure and diffraction pattern with those of the AlFe binary alloy shown in figures 14 and 15.

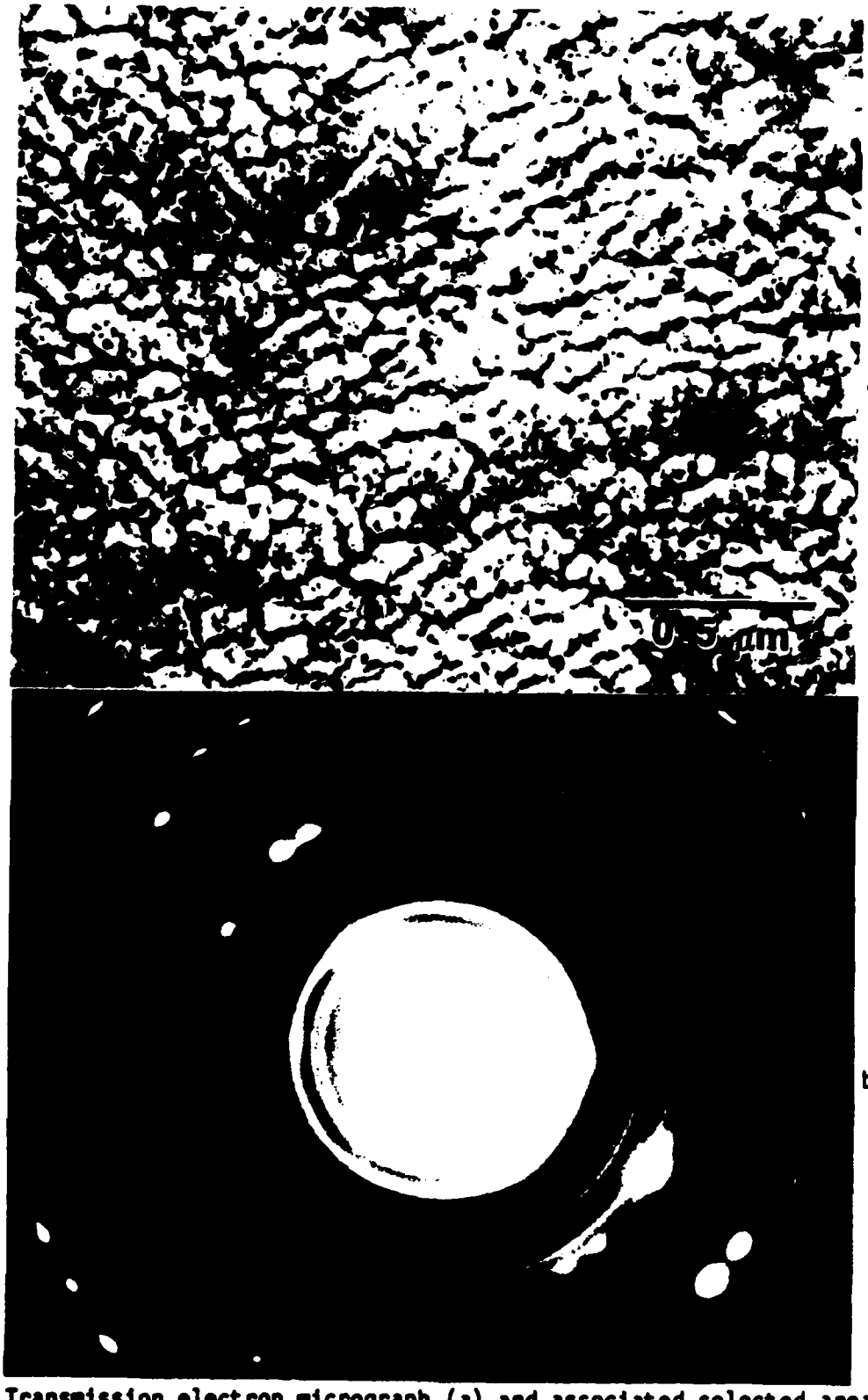

17) Transmission electron micrograph (a) and associated selected area electron diffraction pattern (b) of the laser melted AlFeCe alloy. Note that discreet diffraction maxima can be discerned in the diffracted rings, indicating the presence of larger second phase particles than those observed in the AlFe and AlFeCe alloys.

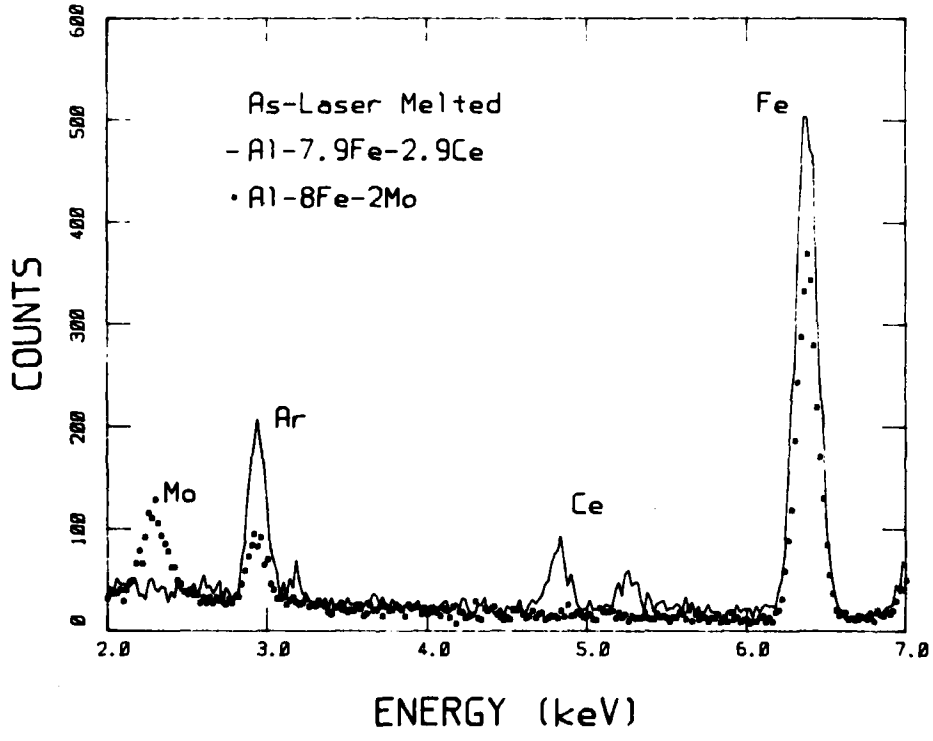

18) Energy dispersive x-ray spectra taken from cells in laser melted AlFeMo and AlFeCe alloys (zone A region). The spectra have been normalized to each other using the AlK peaks (not shown).

Alloy	Composition (at%) Al	Fe	Mo	Ce
AlFe	96.14	3.86	----	----
AlFeMo	97.27	2.13	0.60	----
AlFeCe	96.50	3.11	----	0.39

Table 3. Cell compositions in rapidly solidified alloys

The variation in Fe composition in the cells of the various alloys is interesting, and is shown graphically in Fig. 19, where the Fe-K peaks corresponding to the three alloys are superimposed. (The spectra have been normalized against the Al K peak of the binary alloy).

2.3.2 Microstructures of Heat Treated Alloys

To determine the thermal stability of the various microstructures, rapidly solidified samples of the three alloys have been annealed at 673 K (400°C) for one hour. The resulting microstructures together with representative selected area diffraction patterns are shown in Figs. 20-22, for AlFe, AlFeMo and AlFeCe, respectively. In the case of the binary alloy, AlFe, a number of needle-like phases have formed, and the previously random and continuous rings are now made up of individual diffraction maxima. The needle-like phase is identified as being Al_3Fe, the equilibrium precipitate, and the general decomposition of this zone A microstructure is in accord with the description given by Jacobs, et al.[6].

Inspection of the micrograph and diffraction pattern in Fig. 21, which shows the result of heat treatment of rapidly solidified AlFeMo, leads to the conclusion that very little change has occurred, and this is in marked contrast to the case of the binary AlFe. This is a very significant result and is discussed below in section 2.3.4. Finally, it is evident from Fig. 22 that in the case of the Ce containing alloy, perhaps four phases are present in the microstructure during heat treatment, namely an Al matrix, the unidentified

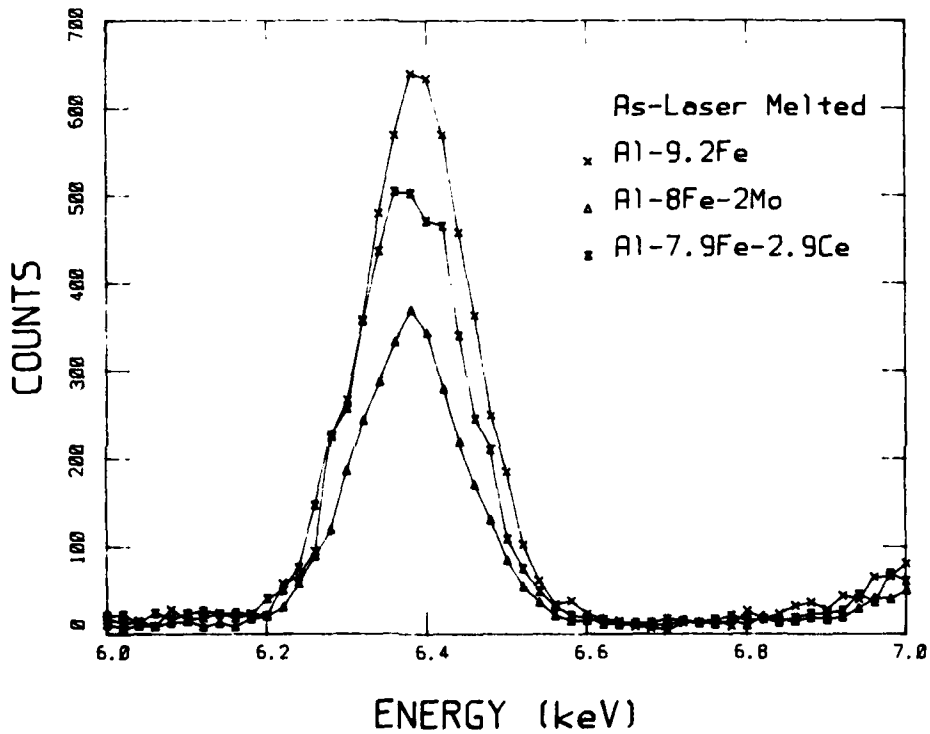

19) Fe Kα peaks from energy dispersive x-ray spectra taken from cells in laser melted AlFe, AlFeMo, and AlFeCe alloys. The spectra have been normalized to each other using the AlK peak (not shown).

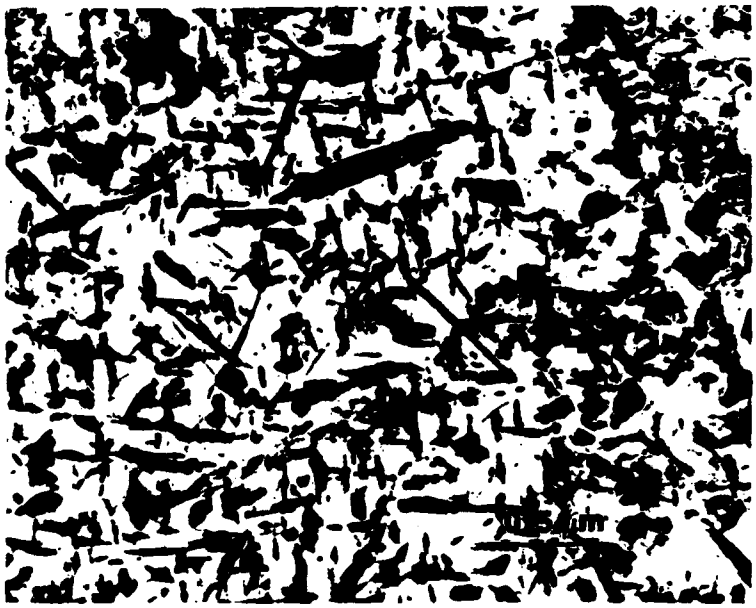

a)

b)

20) Transmission electron micrograph (a) and associated selected area diffraction pattern (b) of laser melted AlFe binary alloy following a one hour anneal at 673°K. Note coarsening of precipitates from the as-solidified condition.

a)

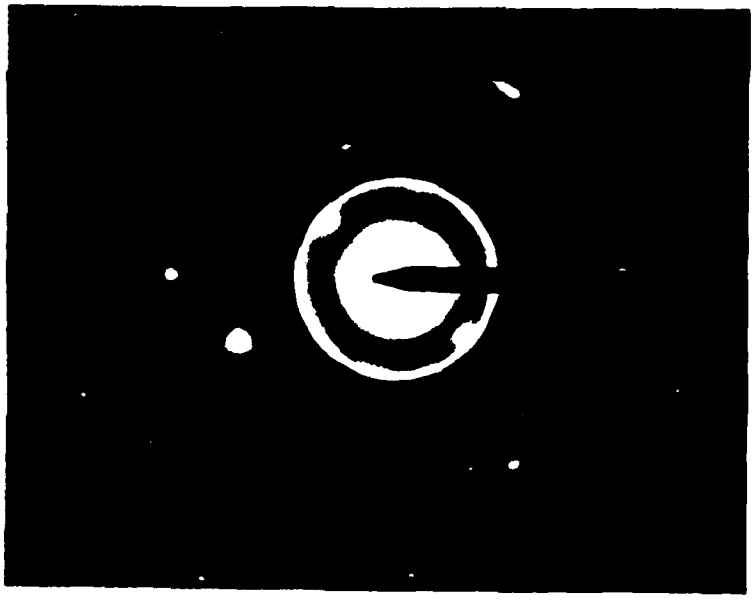

b)

21) Transmission electron micrograh (a) and associated selected area diffraction pattern (b) of laser melted AlFeMo alloy following a one hour anneal at 673°K. Note that little or no coarsening has occurred during annealing.

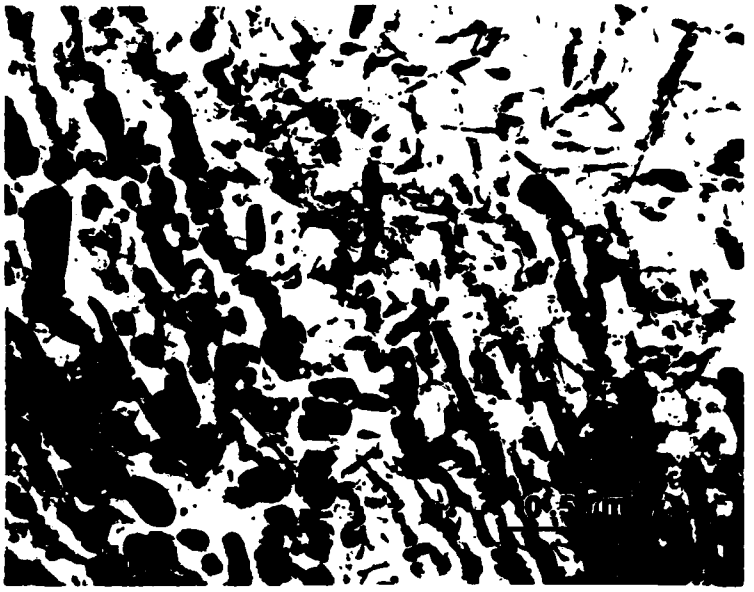

a)

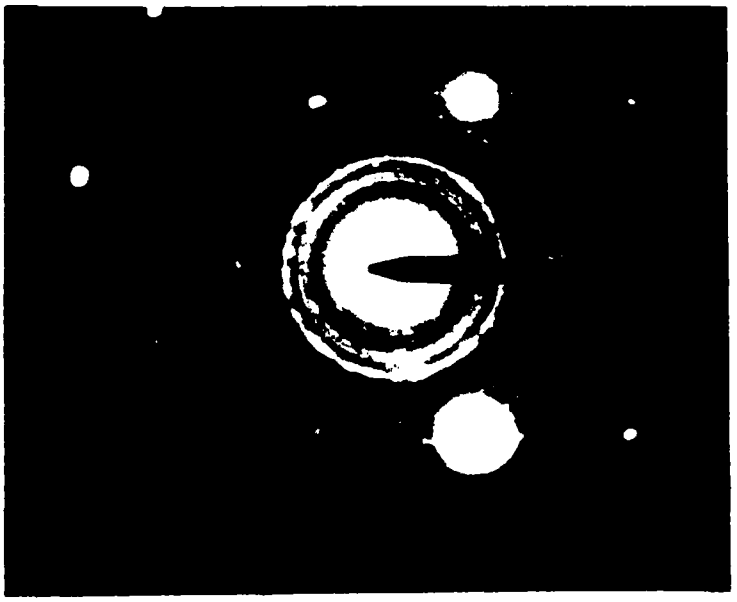

b)

22) Transmission electron micrograph (a) and associated selected area diffraction pattern (b) of laser melted AlFeCe alloy following a one hour anneal at 673°K. Note coarsening of precipitates from the as-solidified condition and the increased number of diffracted rings indicating the presence of additional phases.

phase which is transforming to needles of Al_3Fe, and a set of distinct irregular cylindrical-shaped precipitates. These latter precipitates have not been uniquely identified at this time, but there is some data to suggest that there may be an oxide of Ce, and this possibility is discussed below in section 2.3.4. In summary, it should be noted that heat-treatment of the three alloys at 673 K for one hour leads to quite different microstructures.

2.3.3 Hardness Measurements

Two sets of hardness measurements have been undertaken, the first involving a set of isochronal anneals (for one hour each) at 573 K, 673 K and 773 K for the alloy AlFeMo. The results of these for materials initially in the as-cast condition (denoted "matrix" in the figure) and rapidly solidified (denoted "laser pass" in the figure) are presented in Fig. 23. The alloy in the rapidly solidified condition exhibits reasonable resistance to heat treatment up to ~ 673 K.

The second set of hardness data corresponds to heat treatment at 673 K for various times up to 10 hours. The data for the three alloys, initially in the rapidly solidified condition are shown in Fig. 24. Although the binary alloy exhibits, at first, the highest value of hardness, this drops rather rapidly with annealing time. AlFeMo seems to resist changes in hardness, although an overall decrease is evident after ten hours of annealing. The Ce containing alloy decreases in hardness at an intermediate rate during the initial stages of heat treatment, but then this property becomes relatively unchanged with additional aging.

2.3.4 Discussion

The microstructure of zone A in all three alloys (AlFe, AlFeMo and AlFeCe) consists of a cellular array based on α-Al. This may be understood in terms of the phase diagram[7] shown in Fig. 25. For the composition of 4.7at%Fe, α-Al appears to be the first phase to nucleate, and this implies that there is sufficient undercooling developed to reduce the temperature of the liquid at

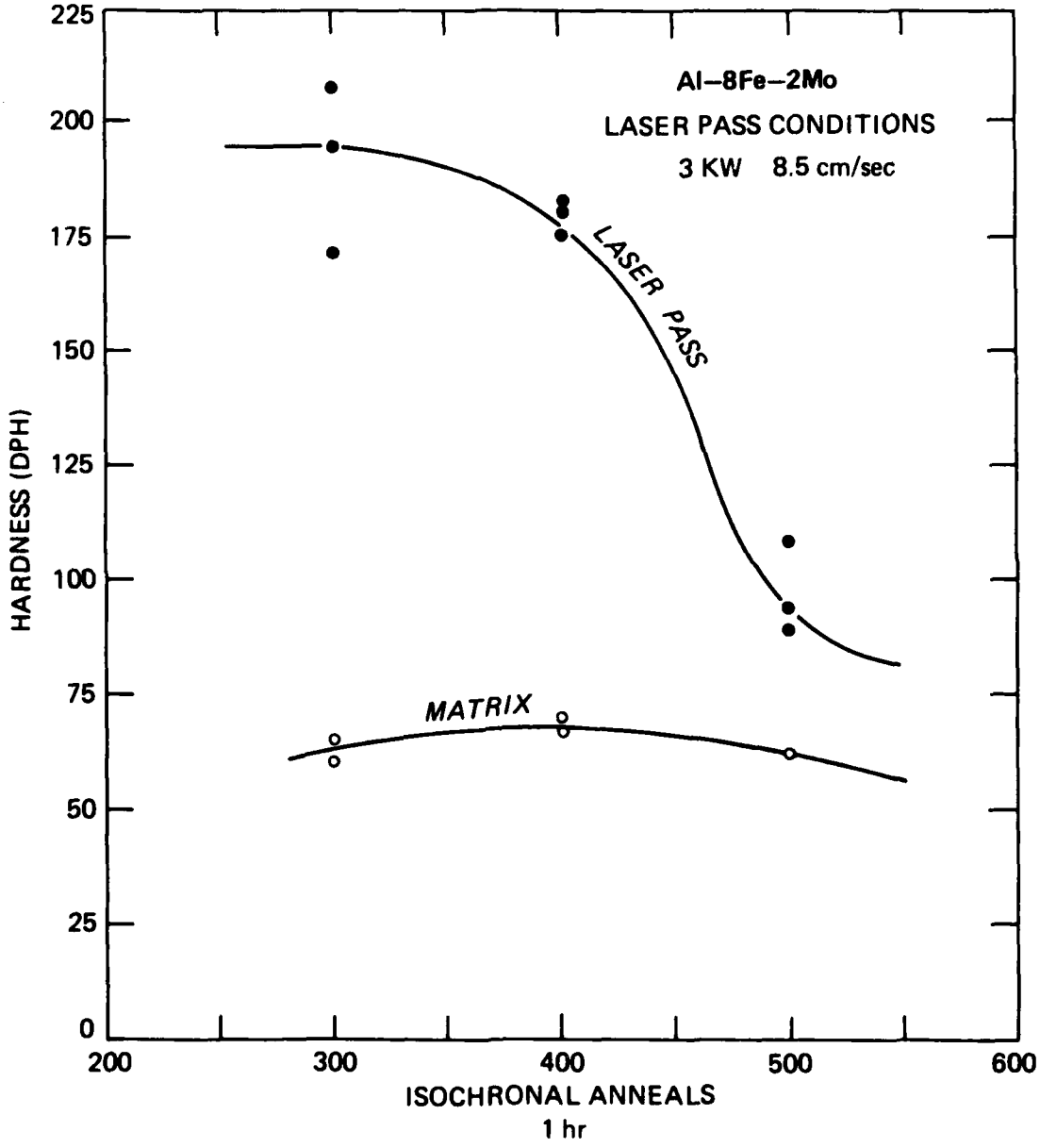

23) Variation of hardness with annealing temperature for laser-melted and as-cast (matrix) AlFeMo alloy.

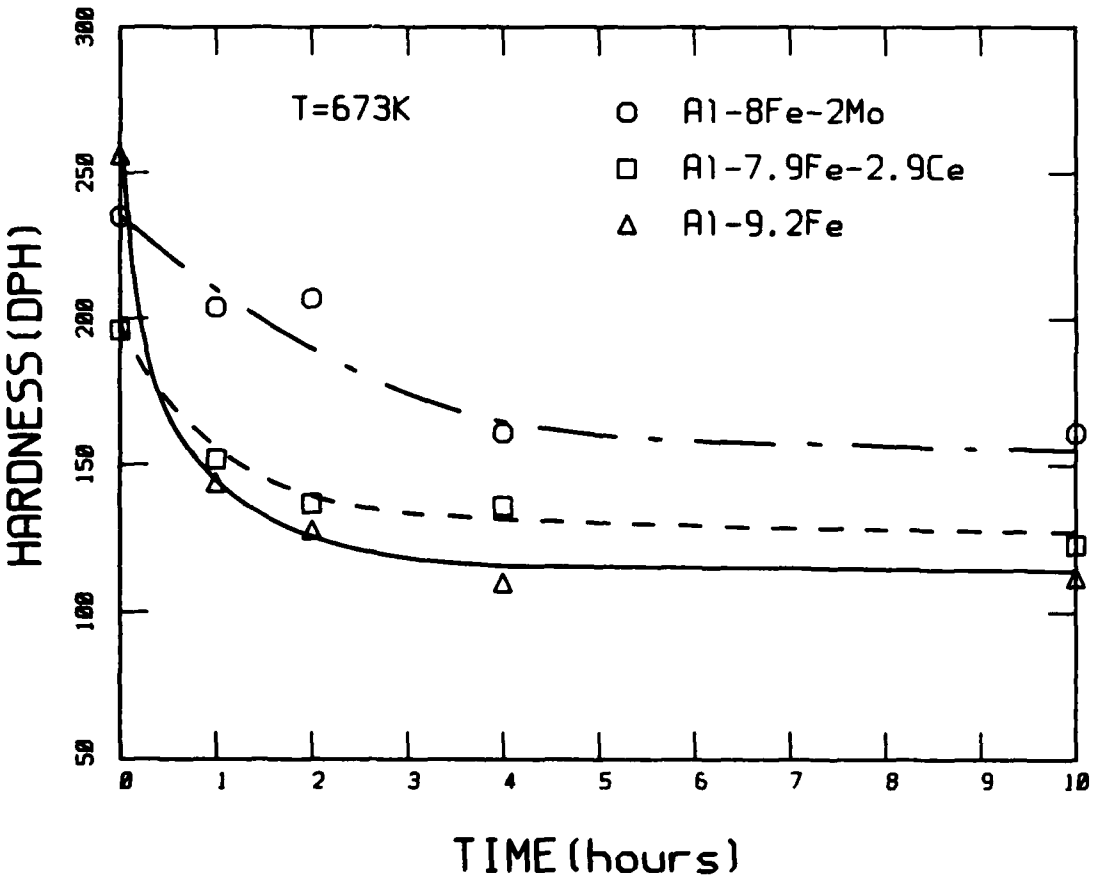

24) Variation of hardness with annealing time (at 673°K) for laser melted AlFe, AlFeMo, and AlFeCe alloys.

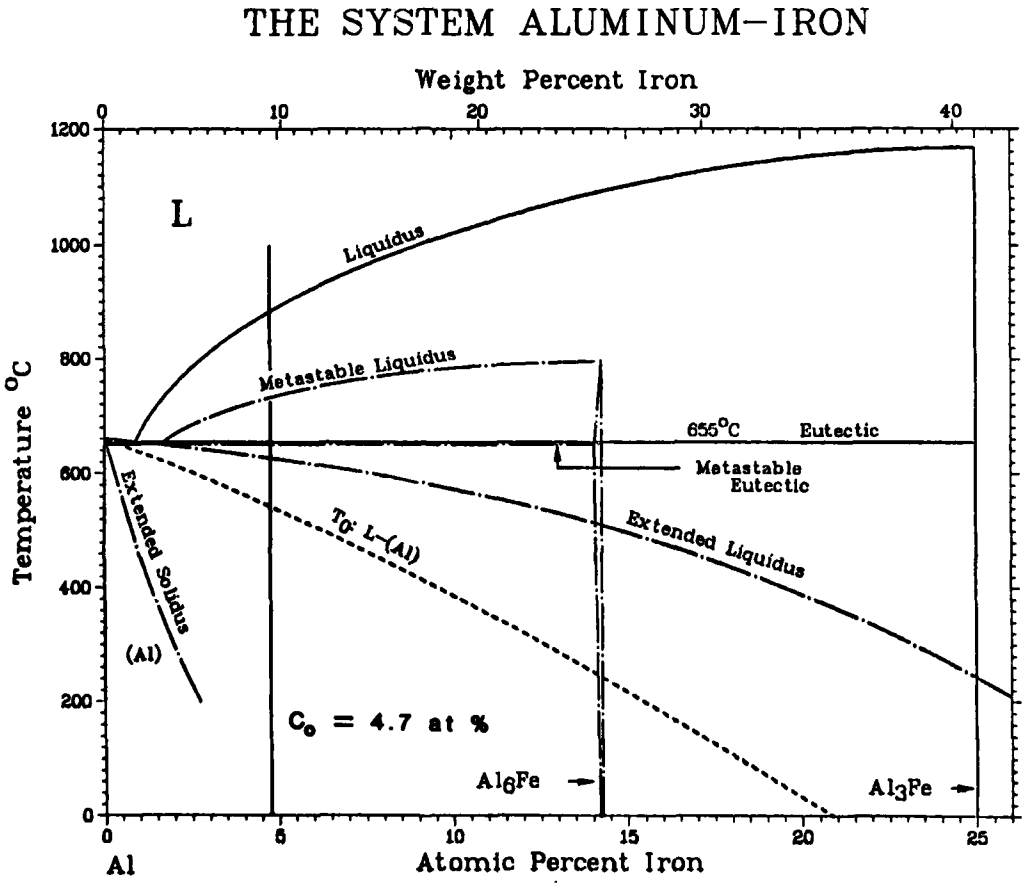

25) Al rich side of the Al-Fe phase diagram showing features of both the equilibrium and metastable diagram. Also depicted on the diagram is the total solute content of the Al-Fe base alloys of this study.

the advancing interface such that it lies below the extended hypoeutectic liquidus curve. According to the phase diagram, an undercooling of ~ 250 K would be required and this value is fairly similar to that which is thought to be developed in the Al-Ni alloys discussed in section 2.1.

The degree to which the α-Al solid solution is supersaturated shows some interesting tendencies. First, the maximum concentration of Fe (3.86 at%) occurs in the binary alloy, and this is also the largest total amount of solute which has been supersaturated in solid solution. The alloy AlFeMo seems to have Mo evenly distributed throughout the microstructure, and so it appears that this element is easily trapped at the advancing interface. However, the amount of Fe found in solution in this alloy is somewhat smaller than that in the binary. Finally, Ce is also found to be trapped in solution in AlFeCe, but to a much lesser extent than Mo in AlFeMo. It appears that Fe and Mo may be relatively easily trapped in the interface, whereas Ce experiences some difficulty. The following reason may be put forward to account for this. It is based on the relative sizes of atoms of these elements compared to that of Al. Table 4 lists the closest distances of approach for atoms of the four elements.

Element	Closest distances of approach (Å)
Al	2.8636
Fe	2.4824
Mo	2.7253
Ce	3.6488

Table 4. Closest distance of approach for the given element (Å)

Mo and Fe are fairly similar in size to Al, albeit slightly smaller. Ce, however, is significantly larger than Al, and it is on this simple and intuitive basis that the difference in trapping efficiency may be explained. Thus, it seems reasonable to assume that atoms of similar sizes, rather than differing sizes, will be more readily absorbed by an advancing interface.

It is interesting to note that the various intercellular second phases in all three alloys are neither Al_6Fe (metastable) nor Al_3Fe, as might be expected from the phase diagram. It is very difficult to obtain unique EDS compositional data from this phase, since the size of the precipitates is simply too small to avoid a large contribution from the matrix to any given EDS spectrum when the electron probe is positioned on the phase. An attempt to obtain such compositional data has been made, using a precipitate that was found to be situated in a very thin part of a foil of the binary alloy. Although this is only an estimate of the composition of the phase, it appears to be consistent with $Al_{12}Fe$. A relatively commonly occurring phase is that based on $Al_{12}W$, but the crystal data from this phase did not fit well with that obtained here for the given intercellular precipitate. The identity of this phase remains unknown.

An inspection of the rings of diffraction maxima in the patterns shown in Figs. 16(b) and (17b) reveals that there are significantly more such rings in the pattern derived from the Ce containing alloy. It is felt that these "extra" rings may well correspond to a second type of intercellular precipitate. The interplanar spacings corresponding to the diameter of these extra rings are tabulated in Table 5. It has been found that the only reasonable fit between these spacings and those of many other candidate compounds occurs for the phase $CeO_{1.67}$, a cubic phase with lattice parameter, a = 11.11 Å. The interplanar spacings and corresponding indices of reflections for this phase are also listed in Table 5.

Unknown Phase	$CeO_{1.67}$	hkl
1.20	1.22	753
1.26	1.28	751
1.43	1.45	731
1.48	1.48	642
1.65	1.67	622
1.79	1.80	611
2.40	2.37	233
2.56	2.54	133
3.34	3.35	113
3.90	3.93	220

Table 5. Interplanar spacings (Å) of reflections in "extra" rings, and those of $CeO_{1.67}$ (with indices of reflecting planes)

The similarity in interplanar spacings between those of the unknown extra second phase in AlFeCe and $CeO_{1.67}$ is quite remarkable, and it may be tentatively assumed that such an oxide phase does exist in the intercellular regions or rapidly solidified alloys containing Ce. However, more confirmatory evidence is required before this may, indeed, be established unequivocally.

It has also been noted that the scale of the intercellular precipitation in AlFeCe is somewhat coarser than that in either the binary or Mo containing alloys. The reasons for this are not, at present, well understood, but a possible explanation is as follows. Thus, the very refined nature of precipitation in AlFe and AlFeMo implies that these phases are nucleated in highly undercooled liquid. This undercooling may be a result of high interface velocities and/or a difficulty in nucleation. The situation in the Ce containing alloys may differ because of the presence of an extra second phase, which may be apparently an oxide, so that either the latent heat of fusion given off by this growing phase may prevent a really high degree of undercooling from occurring, or this phase may provide heterogeneous nucleation sites for the formation of Al/Fe phase. Further work on understanding this difference in scale of precipitation is in progress.

The thermal stability studies yield the remarkable result that the presence of 0.6 at% Mo provides a significant resistance to decomposition of the zone A microstructure. It appears that the presence of uniformly distributed Mo atoms causes a marked reduction in the diffusivity of Al. The mechanism that would cause this effect is not known at present.

Finally, there are a number of interesting features exhibited by the hardness curves presented in Fig. 24. Hardness is related somewhat to the strength of a given material, and so variations in hardness reflect changes in strength which are presumably caused by microstructural differences. In the present case, it is felt that there are three major contributing aspects of the microstructure that give rise to the apparent high hardnesses of these alloys. First, the zone A microstructure consists of a set of very small cells, ~ 0.1 μm in cross section. Secondly, there is an extremely refined dispersion of intermetallic phases at the intercellular regions. Finally, there is considerable supersaturation of solute atoms in the α-Al cells, so that there is a strong element of possible solid solution strengthening. In the rapidly solidified condition, the binary and AlFeMo alloys exhibit the highest hardness, whereas that of the AlFeCe alloy is considerably lower. This observation implies that an extremely significant element of strengthening is that involving the very refined distribution of precipitates in the intercellular regions, since all three alloys have a cellular structure of approximately the same scale and a fair amount of solute in solid solution. On aging at 673 K, the hardness of the binary alloy drops rapidly, and it is found that the zone A microstructure of this material also has decomposed significantly. However, the Mo containing alloy appears to retain a relatively high hardness, and it is seen that its microstructure appears to be essentially unaffected. This again emphasizes that it is the presence of the extremely refined dispersion of intermetallic compounds which makes a major contribution to the strength of the alloy. The alloy AlFeCe also decreases in hardness on

aging but not to the same extent as the binary alloy. Inspection of this material in the aged condition shows that although the microstructure has decomposed from that of zone A, it is rather different from the case of the aged binary alloy, and exhibits a relatively uniform dispersion of the second phase, tentatively identified as an oxide, which presumably accounts for its intermediate hardness level.

3. Production of Rapidly Solidified Powders

The laser spin atomization (LSA) technique has been used to produce powders of the alloy Al-0.5at%Mo. A scanning electron micrograph of these powders is shown in Fig. 26. The sizes range from ~ 10μm to 400 μm, the average being ~ 95 μm. The surface of one of these powders is shown in Fig. 27, using the backscattered electron compositional mode in the scanning electron microscope. It is clear from this micrograph that the surfaces contain a large number of large second phase precipitates. This is not an encouraging result, since it is hoped to produce a refined distribution of phases following rapid solidification. When the powders are mounted and sectioned, and then studied in the scanning electron microscope using the compositional mode, micrographs such as that in Fig. 28 result. Here, it is clear that the amount of these second phases varies from powder to powder. Thus, the composition and microstructure of the powders are not constant. The reason for this must be due to the insufficient superheat generated in the molten alloy at the tip of the spinning ingot prior to atomization. Presumably the α-Al matrix melts first, and before the second phase also melts, this liquid is ejected in the form of droplets. In this way, the number of unmelted precipitates in each powder may vary considerably. Clearly, the LSA technique is not suitable for alloys such as Al-Mo, where there is a very wide range over which the various components of the microstructure melt. For future work, emphasis is being placed on two methods of producing particulate, one involving

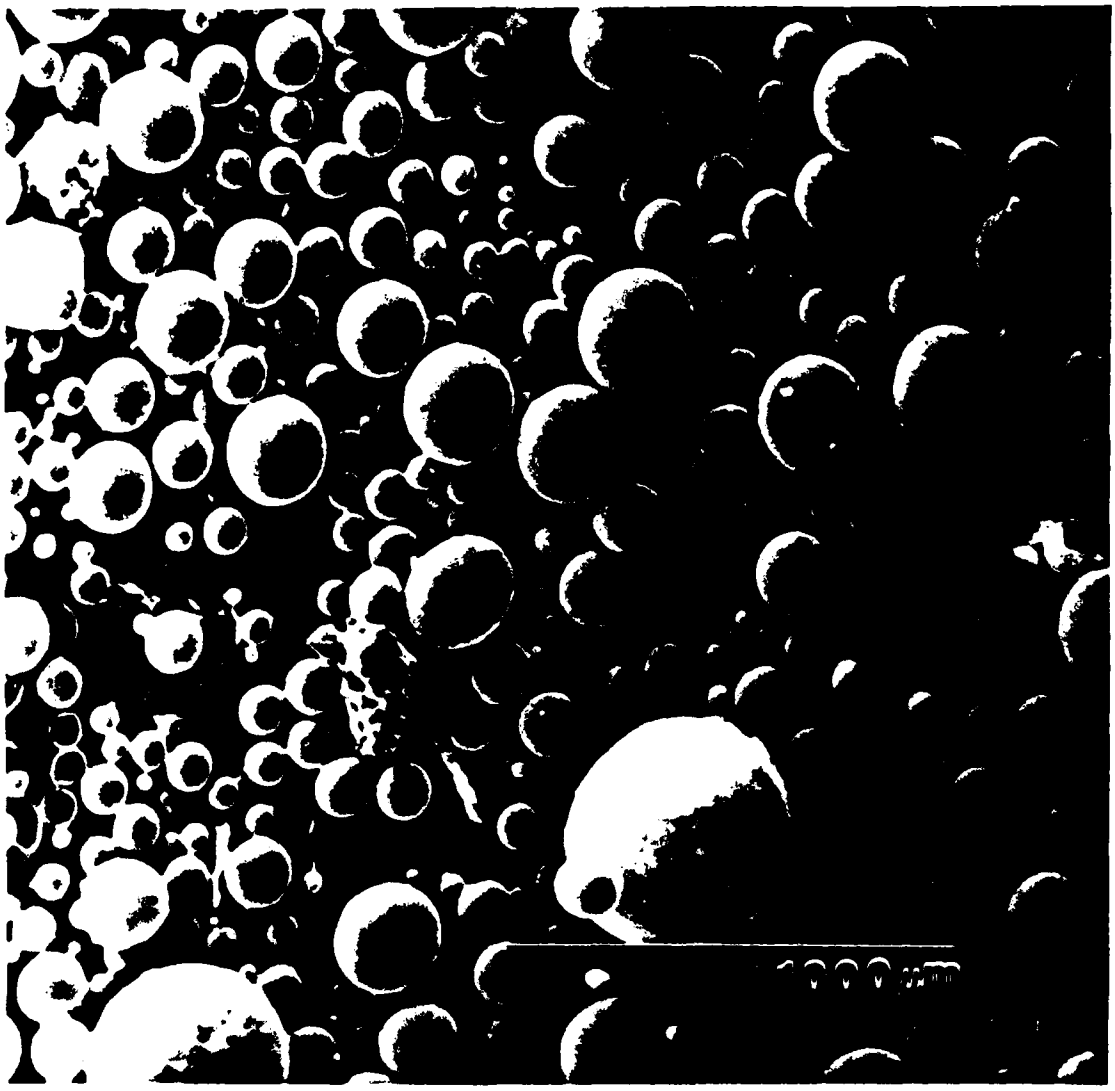

26) Secondary electron image of Al-0.5at%Mo powder produced by laser spin atomization.

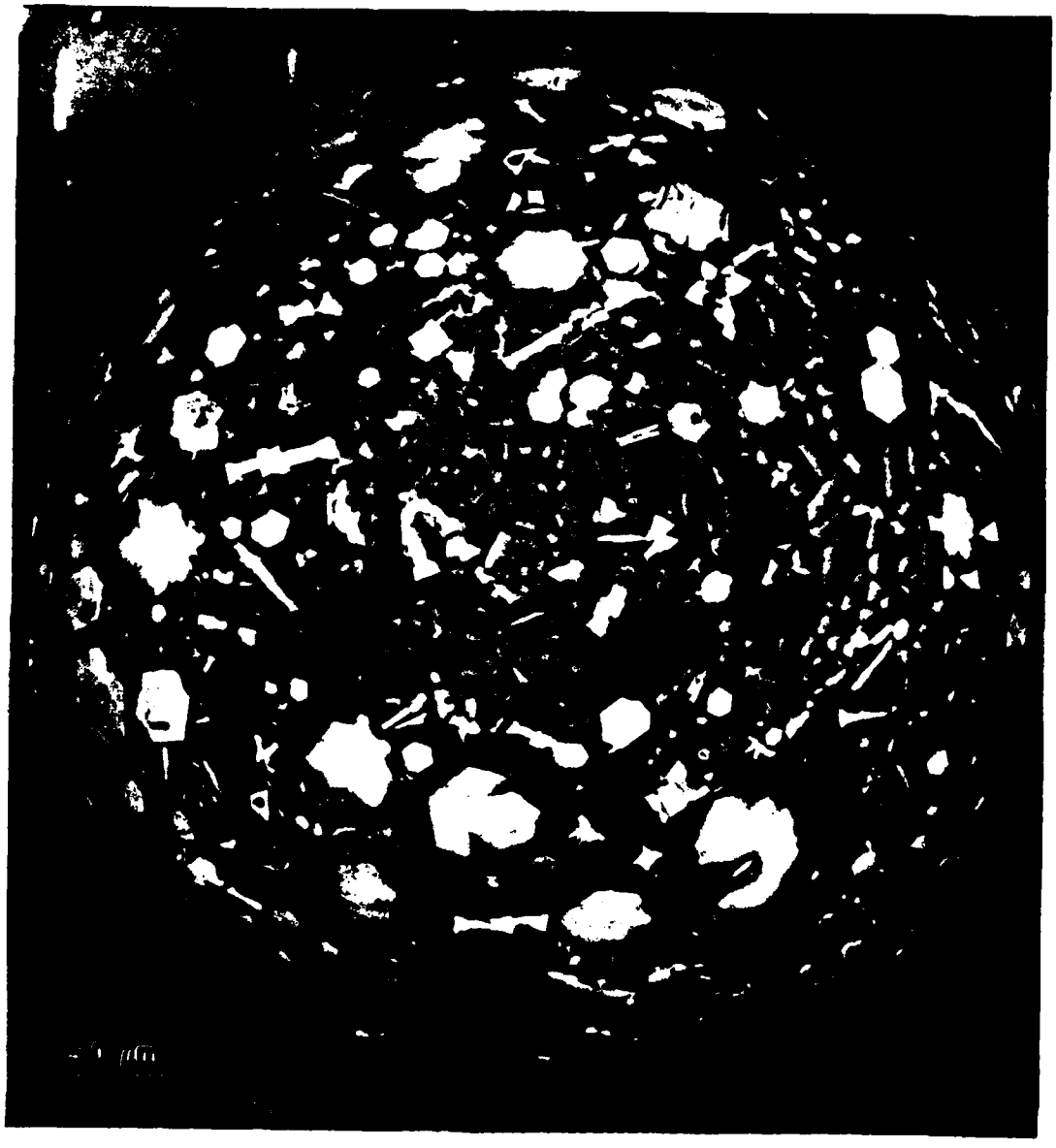

27) Compositional back-scattered electron image of a single Al-0.5at%Mo powder particle produced by laser spin atomization. Note the presence of second phase particles.

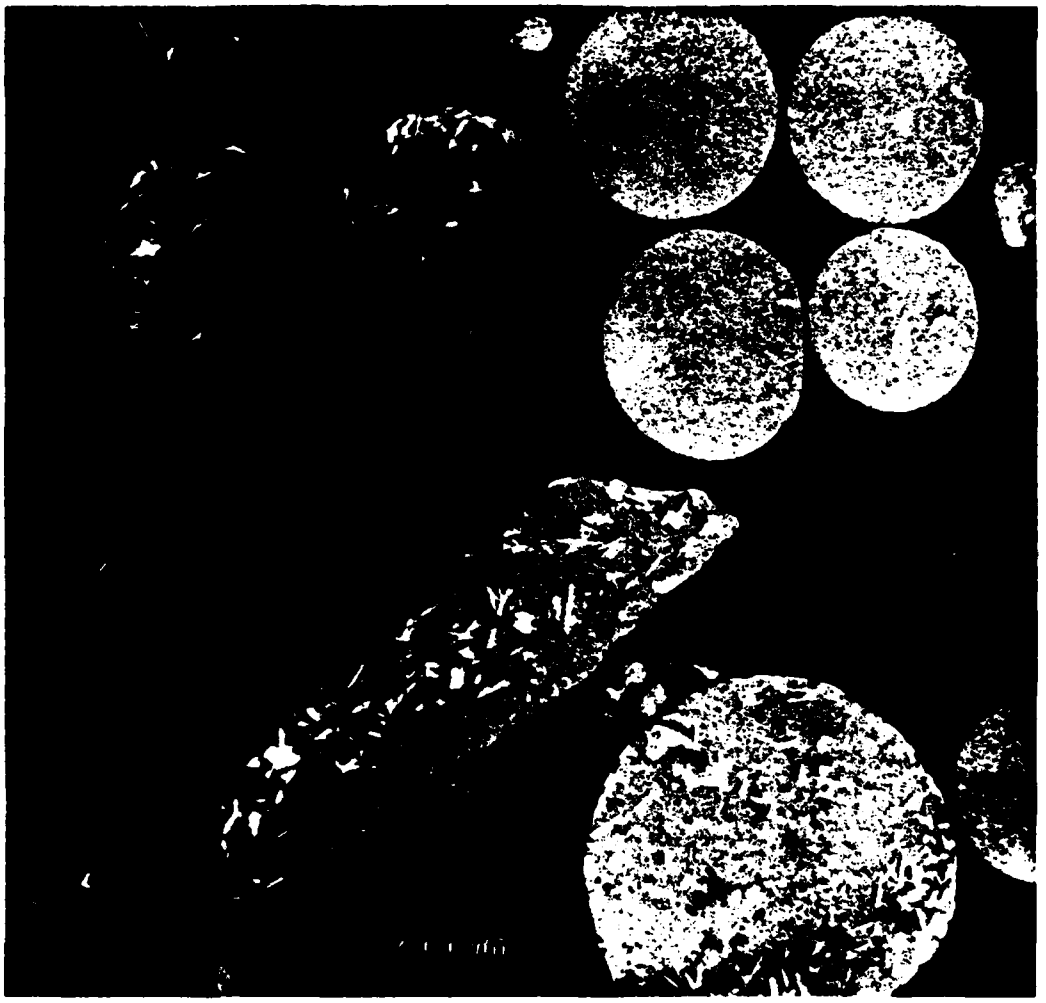

28) Compositional back-scattered electron image of Al-0.5at%Mo powder produced by laser spin atomization, shown in cross-section. Note the uneven distribution of precipitates between the powder particles.

centrifugal atomization and the other melt-spinning. In the case of the latter, the ribbon will be reduced to particulate using one of several methods now under investigation. The advantage to this approach, i.e. melt-spinning and subsequent reductions of ribbon to particulate lies in microstructural control. Thus, it has been shown in section 2 that materials which possess zone A microstructures exhibit high hardnesses, and, therefore, strengths. Also, it has been shown that the production of zone A microstructures depends on a high degree of undercooling being developed in the melt. In practice, it seems more simple to achieve reproducible solidification conditions in ribbon rather than powders in which the degree of undercooling is a function of particle diameter. An example of a ribbon of Al-3at%Fe-0.6at%Mo which possess zone A microstructure is shown in Fig. 29.

4. Dynamic Compaction of Rapidly Solidified Powders of 7091

Despite the fact that in many instances much trouble is taken to prepare rapidly solidified particulate possessing refined and sometimes metastable microstructures, often the consolidation process involves prolonged thermal excursions so that microstructural coarsening occurs. A part of the present program involves a study of the possible consolidation of rapidly solidified Al alloy particulate using dynamic powder compaction (DPC). In this process, a high velocity projectile is caused to be incident on a set of powders, and consolidation is affected by the passage of the resulting shock wave through the particulate assembly. Consolidation is thought to occur by local melting of the powder surfaces, so that subsequent self-quenching by the particulate interiors rapidly solidifies these liquid regions. Therefore compaction occurs without the application of a prolonged thermal excursion. The present set of experiments made use of powders of 7091, produced by ALCOA using gas atomization. The samples were kindly supplied by Dr. H. Gegel of AFWAL/ML. The alloy composition is nominally Al-6.5Zr, 2.5Mg, 1.5Cu, 0.4Co (compositions in wt%).

29) Optical micrograph of Al-3at%Fe-0.6at%Mo melt-spun ribbon, sectioned along the ribbon length, transverse to the heat flow direction. Note the absence of contrast within the ribbon indicating an all zone A microstructure.

The microstructures and shapes of the as-received powders are shown in Figs. 30 and 31, respectively. The microstructures appear to be of a dendritic/cellular nature. The shapes are rather irregular, a highly desirable feature of pwoders to be compacted. Powders were consolidated using the light gas gun developed for DPC purposes by the research group of the P.I. at the University of Illinois. An example of 7091 powders compacted in this way is shown in Fig. 32. Although some light surface cracking is visible, generally the compacts are of good integrity. In our apparatus, a convenient process variable is the incident projectile velocity, and the dependences of compact hardness and density on this parameter have been determined. These are shown graphically in Figs. 33 and 34, respectively. The hardness is seen to increase monotonically with velocity, and this presumably reflects the increase in stored energy resulting from the severe plastic deformation of the material caused by the propagating shock wave. The density is also seen to be a function of projectile velocity, and reaches approximately theoretical density at the more rapid velocities.

An optical micrograph of dynamically compacted 7091 powders is shown in Fig. 35. The density of this compact was determined as being ~ 97% (of theoretical density), and this high degree of compaction is evident from this micrograph. However, density is a necessary but not a sufficient criterion for a "good" compact. Thus, the production of good metallurgical bonds between the particulate is also required, and in this respect the micrograph presented in Fig. 36 involves an interesting observation. A crack is visible in the compacted material, and it can be seen that the crack propagates through a pre-existing dendritic powder rather than along the adjacent prior particle boundaries. Certainly this is consistent with the development of metallurgical bonds between particles.

Thin foils of dynamically compacted powders have been prepared and the microstructure has been characterized thoroughly using analytical transmission

30) Optical micrograph of gas atomized 7091 powder used in dynamic compaction experiments, shown in cross-section.

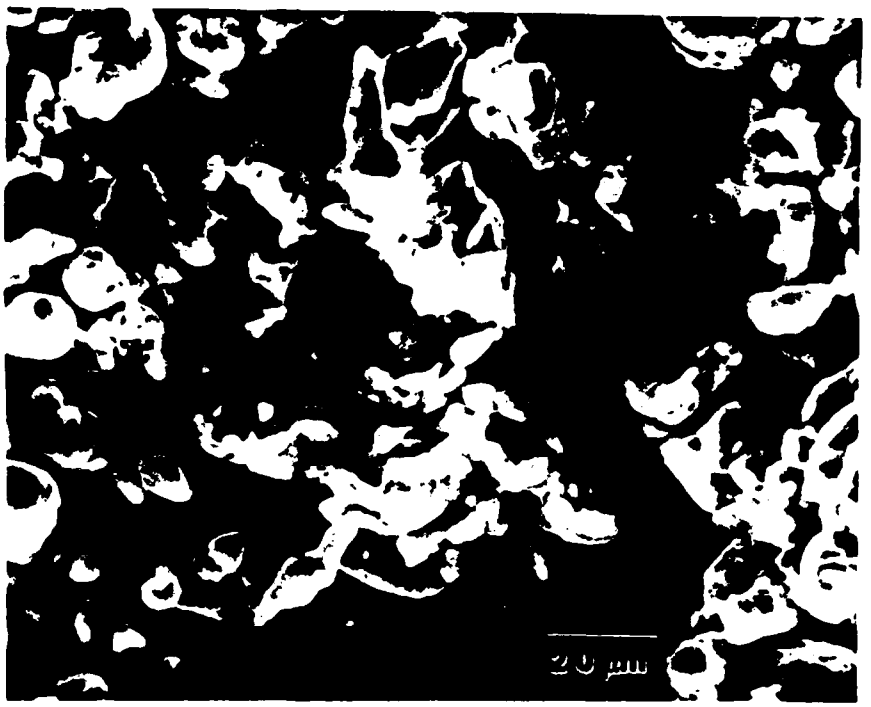

31) Secondary electron image of gas atomized 7091 powder used in dynamic compaction experiments.

a)

a

1.0 cm

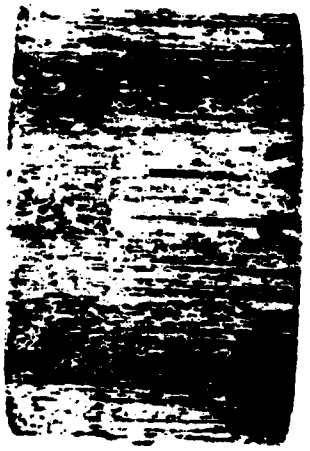

b)

b

1.0 cm

32) Photomicrograph of dynamically compacted 7091 powder specimen shown with compaction direction
a) normal to the page, b) parallel to the page (horizontal).

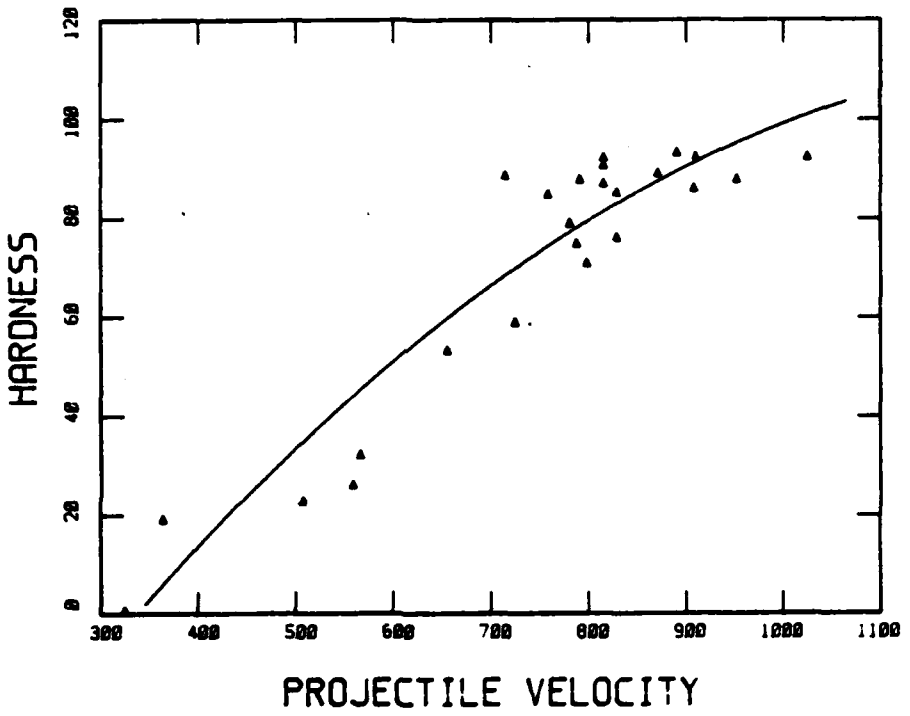

33) A plot of specimen hardness as a function of projectile velocity (m/s), showing data for dynamically compacted 7091 powder and fitted curve.

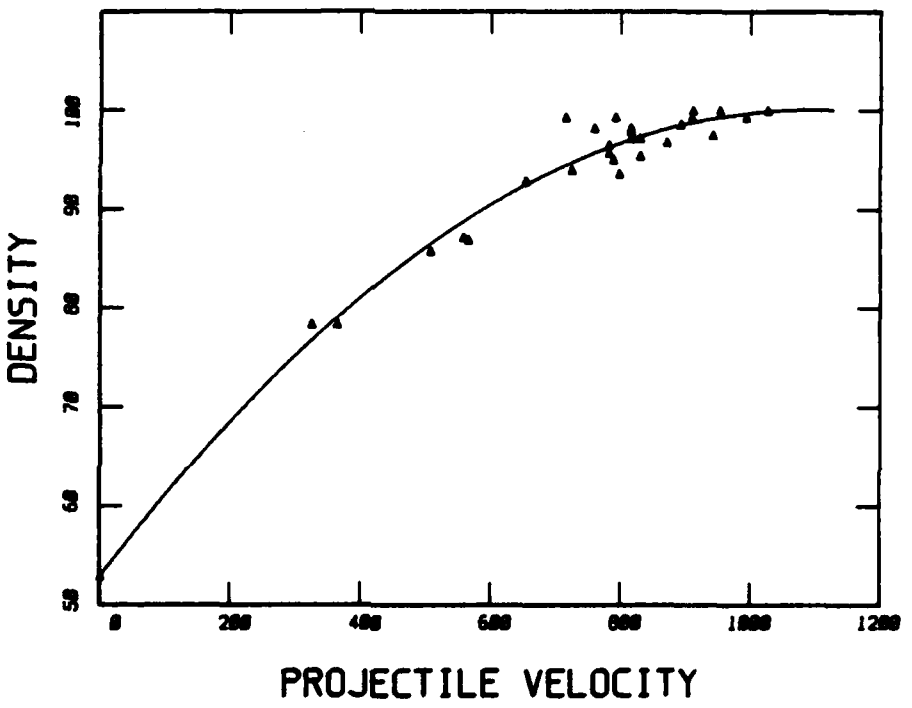

34) A plot of specimen density as a function of projectile velocity(m/s), showing data for dynamically compacted 7091 powder and fitted curve.

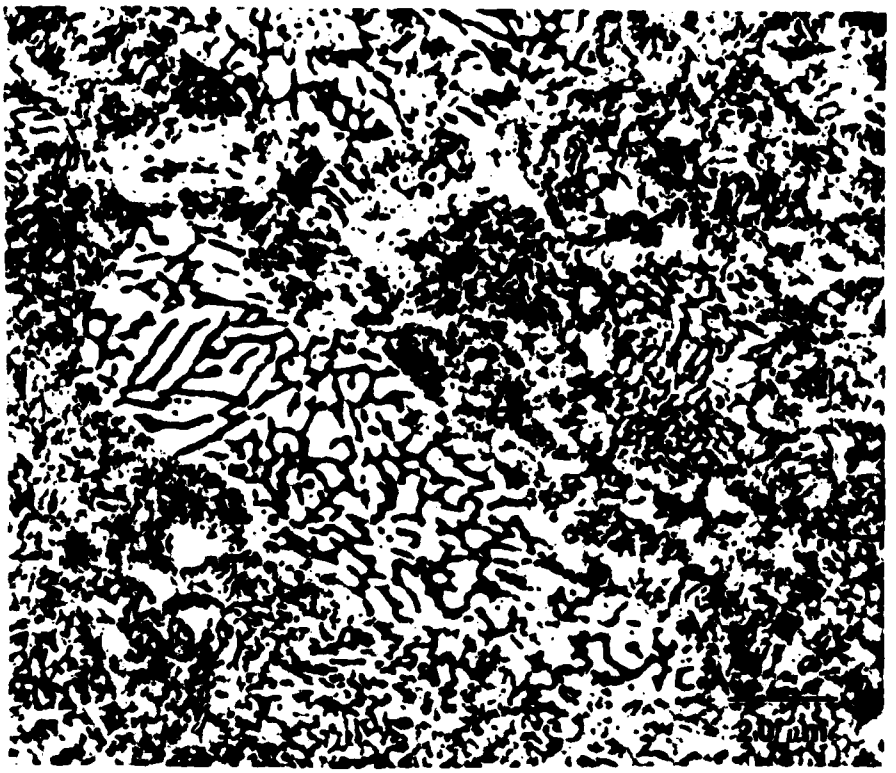

35) Optical micrograph of 7091 powder dynamically compacted using a gas pressure of 1600 psi.

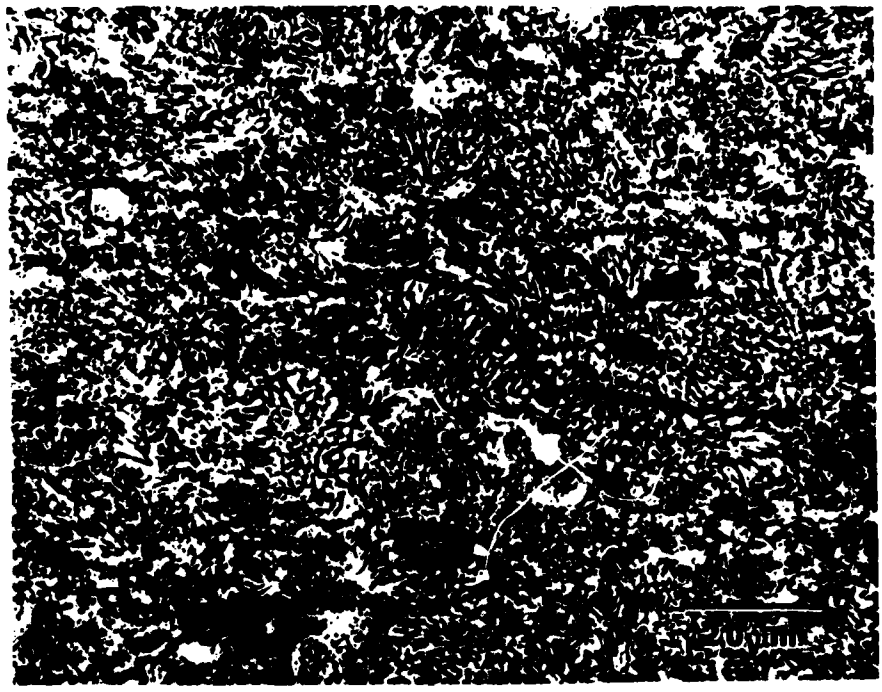

36) Optical micrograph of dynamically compacted 7091 powder. Note that the crack has propagated through the powder particle rather than along the prior particle boundaries.

electron microscopy. Of particular interest in the present study is the mechanism of compaction, and so much emphasis has been placed on the microstructure of the prior particle boundaries. Two such boundary regions are shown in Fig. 37(a) and (b). In the first of these, it is evident that the dendritic structure of the cell interior has been modified in the boundary region. For example, there are terminations in dendrite arms at finite distances from the actual boundary, and it is tempting to speculate that this may indeed be the result of local melting. In Fig. 37(b), a series of small precipitates has formed along a boundary region and these particles resemble those formed during heat treatment (see Fig. 39 below). The identity of these small precipitates is not known, but a comparison of the EDS spectra recorded form the interdendritic phase and these small particles may be made in Fig. 38. Thus, the small particles appear to be richer in Fe, Co, Cu and Zn compared to the interdendritic phase.

The surfaces of gas atomized Al powder are known to possess a rather adherent layer consisting of an hydrated oxide. In the present study, no attempt was made to remove these layers by the application of heat prior to consolidation, so that it is of interest to determine whether on subsequent heat treatment, this pre-existing layer might give rise to cavities or voids in the compacts. Two temperatures were chosen for this heat treatment, namely 523 K and 732 K. Fig. 39 is a TEM micrograph of a thin foil taken from a compact which had been annealed at 523 K for one hour. The dendritic microstructure of the as-compacted material has decomposed, and small precipitates have formed. The EDS spectrum recorded from a particle (Fig. 40(a)) is shown to be rich in Zn together with small amounts of Cu and Co. The matrix (Fig. 40(b)) is seen to be basically Al, with small quantities of Zn, Cu and Co present. Aging at 723 K results in a quite different microstructure, such that two types of precipitate form, one approximately spherical in shape, the other rod-like, see Fig. 41. The EDS spectra shown in Fig. 42 reveal that the spherical particles

a)

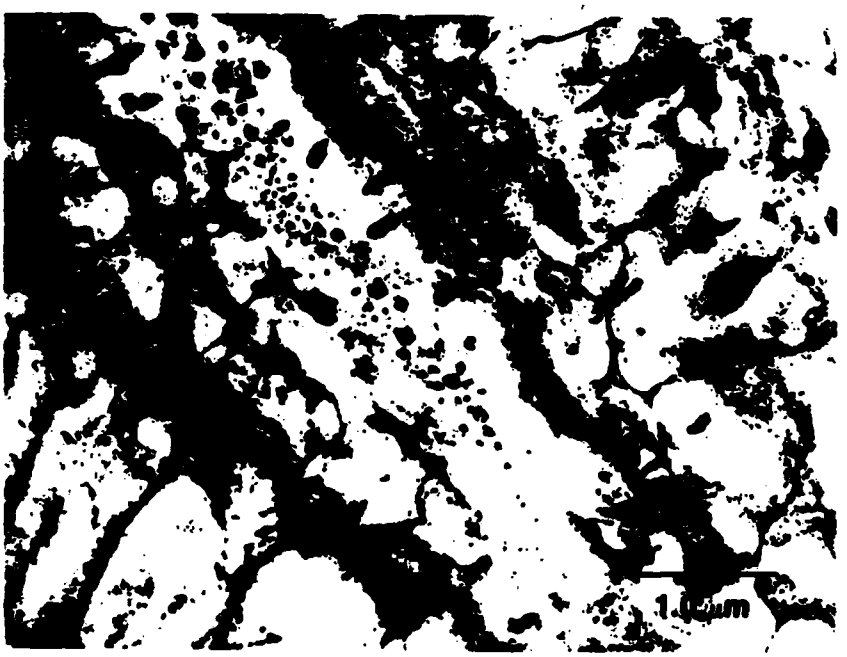

b)

37) Transmission electron micrographs of dynamically compacted 7091 powder, showing prior particle boundaries. Note the termination of dendrite arms at a finite distance from of the boundary (a) and the presence of precipitates in the boundary region which resemble those seen in the heat treated specimens shown in figure 39 (b).

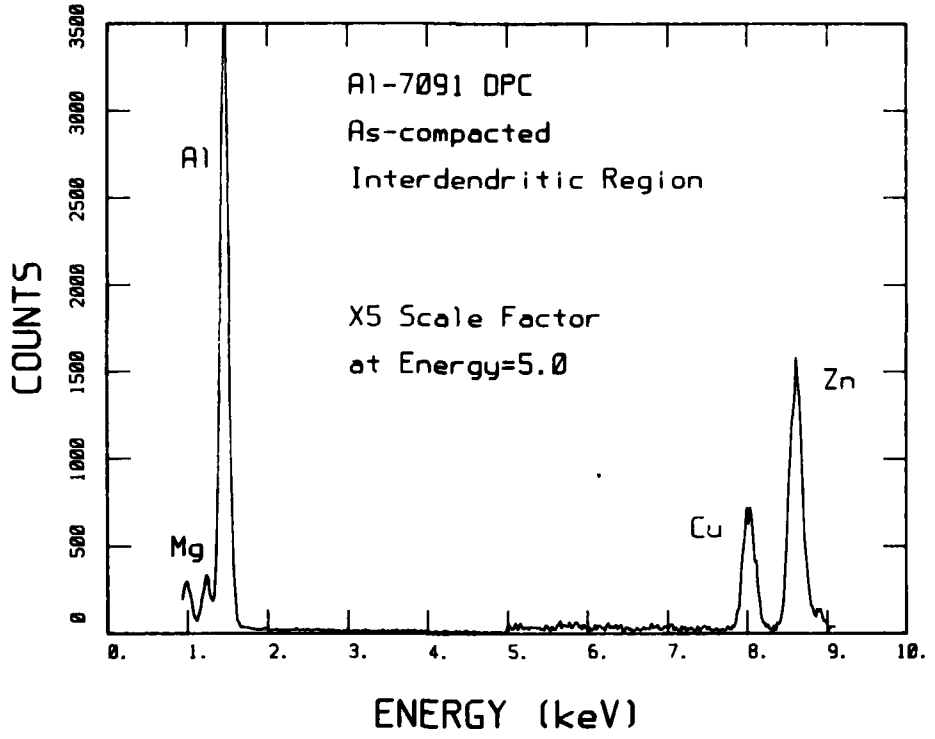

a)

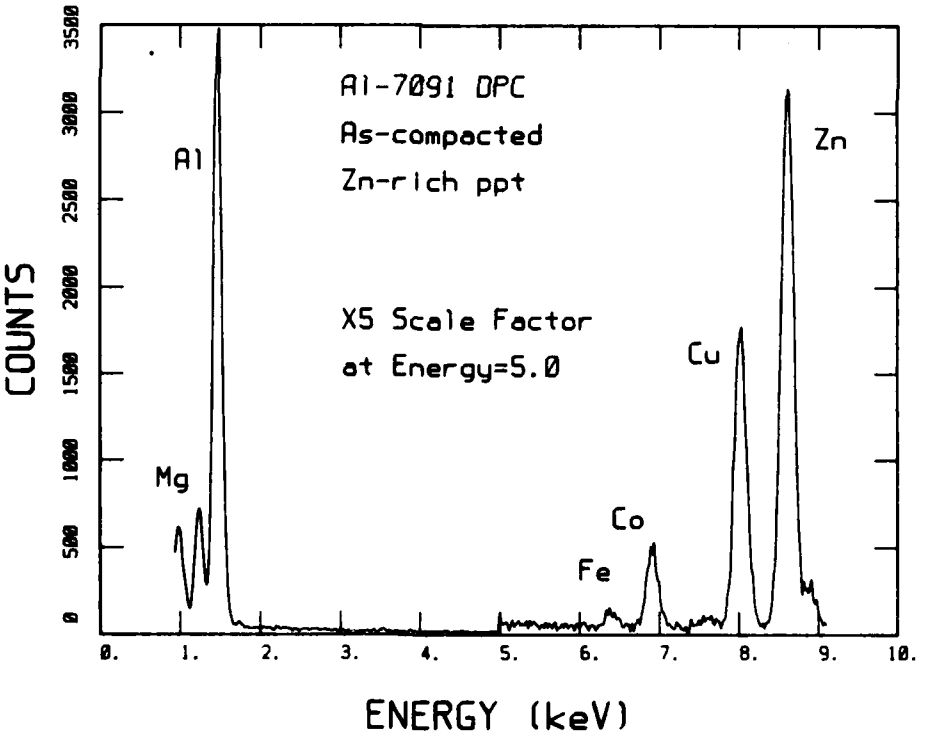

b)

38) Energy dispersive x-ray spectra taken from as compacted 7091 powder
a) interdendritic region
b) small precipitates found in the prior particle boundary region (shown in figure 37b)

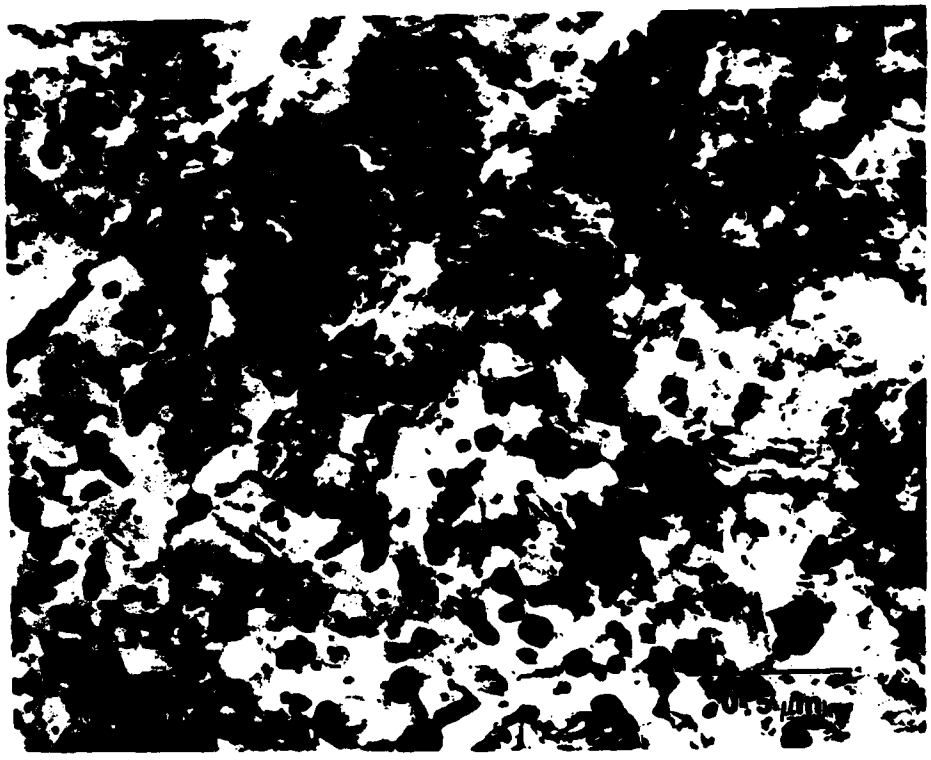

39) Transmission electron micrograph of dynamically compacted 7091 powder following a one hour anneal at 523°K.

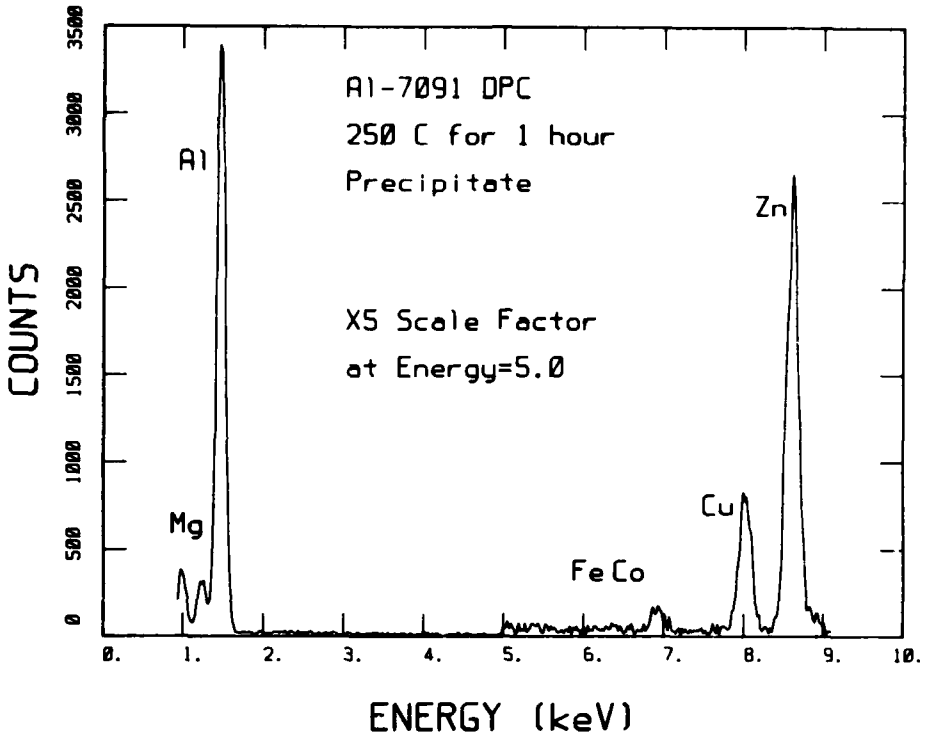

a)

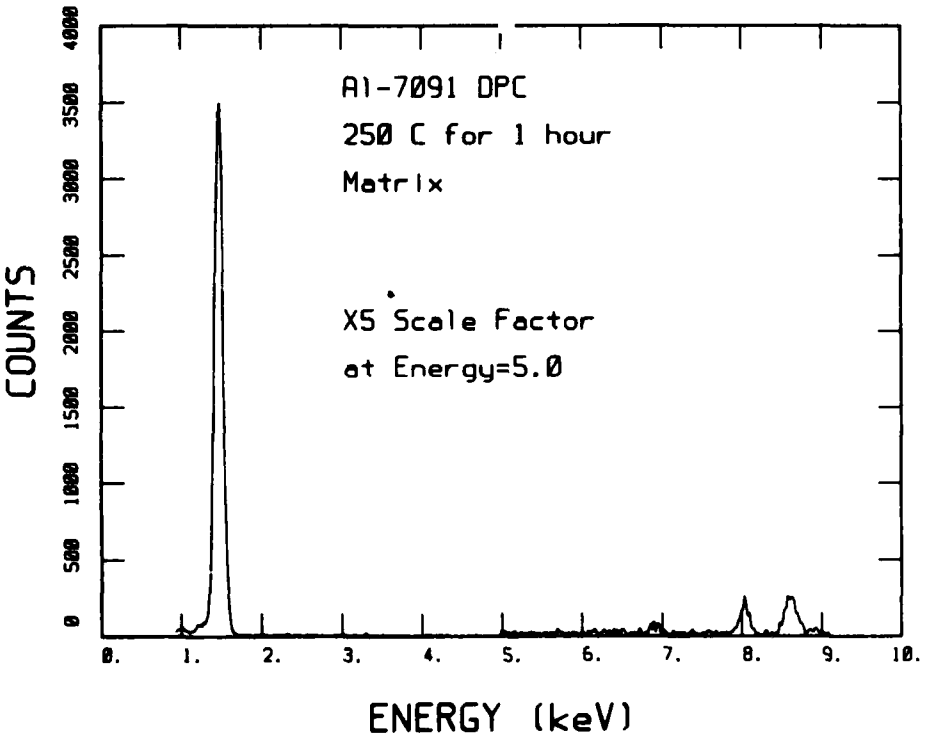

b)

40) Energy dispersive x-ray spectra from the specimen shown in figure 39
a) taken from precipitate
b) taken from matrix.

41) Transmission electron micrograph of dynamically compacted 7091 powder following a one hour anneal at 723°K.

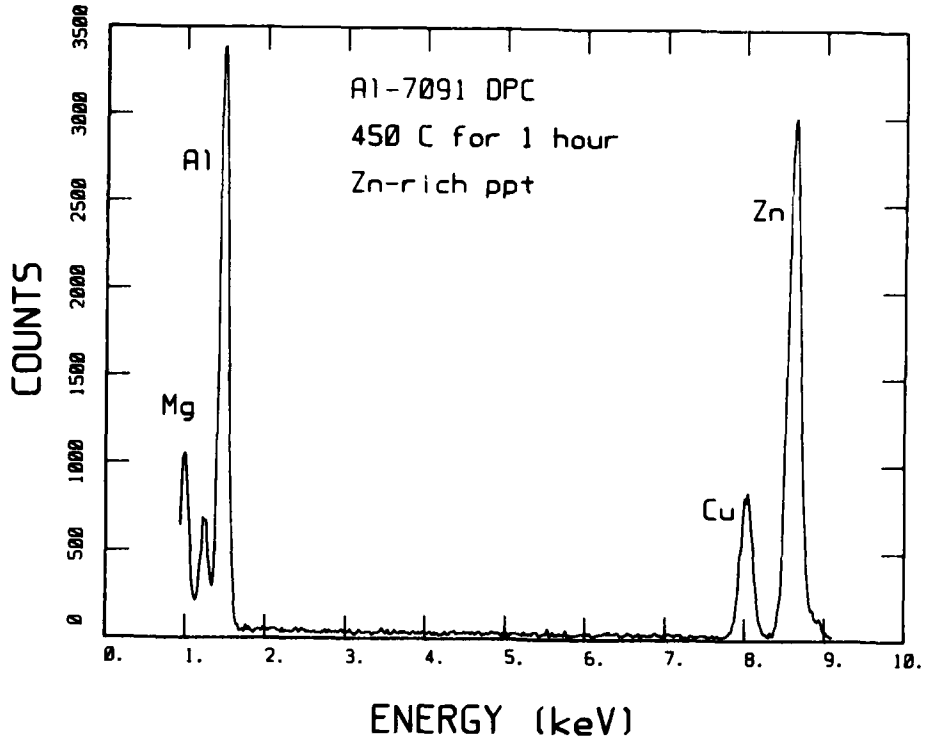

a)

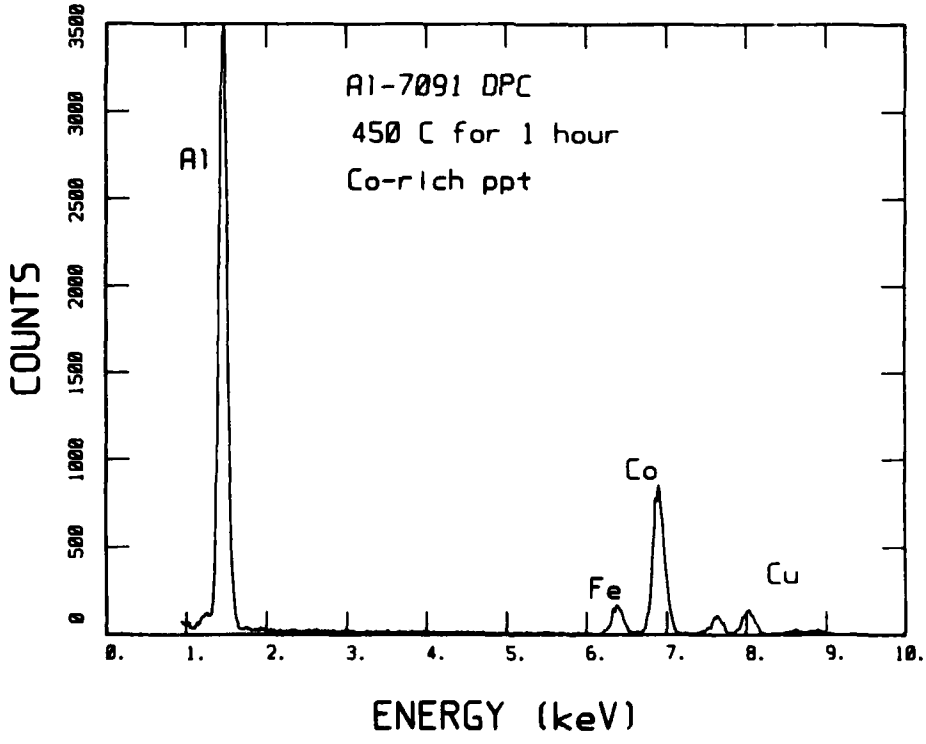

b)

42) Energy dispersive x-ray spectra taken from two precipitates in the specimen shown in figure 41
    a) rod-like precipitate
    b) spherical precipitate.

are rich in Co and Fe, and are probably $(Co,Fe)_2Al_9$, whereas the rod-like precipitates are rich in only Zn and Cu. The identities of all these various phases in these samples are not well established at present, however this will be accomplished during future work. It should also be pointed out that no cavitation or void formation as a result of heat treatment has been observed. The dispersion of the hydrated oxide layer during shock consolidation is not understood and is a subject of current study.

The present set of experiments is extremely encouraging in terms of compaction of rapidly solidified powders of Al alloys. It is now hoped that during the next contract year that particulate with tailored microstructures (e.g. zone A) will be produced and compacted in this way.

5. References

1. H. Jones, 1969/70, Mater. Sci. Eng. 5, 1

2. W.J. Boettinger, 1982, "Rapidly Solidified Amorphous and Crystalline Alloys", eds. B.H. Kear, B.C. Giessen and M. Cohen, Elsevier Science Publ. Co., p. 15

3. A.F. Polesya and A.I. Stepina, 1970, Fiz. Metal. Metalloved., 30, 929

4. B.F. Buxton, J.A. Eades, J.W. Steeds and G.M. Rackham, 1976, Phil. Trans. Roy. Soc. London, A281, 171

5. G. Thursfield and M.J. Stowell, 1976, J. Matls. Sci., 9, 1644

6. M.H. Jacobs, A.G. Doggett and M.J. Stowell, 1974, J. Matls. Sci., 9, 1631

7. L. Swartzendruber and J. Murray, 1983, Bull. Alloy Phase Diags., in press

Publications

"Microstructural Characterization of Rapidly Solidified Materials", H.L. Fraser and J.B. Vander Sande, Proc. Third Conference on Rapid Solidification Processing Principles and Technologies, III, NBS Special Report.

END

FILMED

11-83

DTIC